# CAR–PARRINELLO METHODS IN CHEMICAL ENGINEERING: THEIR SCOPE AND POTENTIAL

**Bernhardt L. Trout**

**Department of Chemical Engineering, Massachusetts Institute of Technology, Cambridge, Massachusetts 02139**



## I. Introduction

It is now 15 years after the publication of the famous paper by Roberto Car and Michele Parrinello (1985) on the integration of the quantum mechanical method, density-functional theory, with classical molecular dynamics. By





ADVANCES IN CHEMICAL ENGINEERING, VOL. 28 0065-2377/01 $35.00

Moore's law, computational power has increased by a factor of 1000 since then. In addition, with the development of many computer codes that employ the Car–Parrinello method, combined with the enhanced accuracy of density functionals that have been devised since 1985, there has been widespread use of the Car–Parrinello method. Between 1997 and the beginning of 2000, over 500 papers that incorporate results found using Car–Parrinello simulations have been published in major journals. Most of these papers have been published by groups considered primarily to be in the field of physics. On the other hand, the topics of these papers span the spectrum of disciplines as traditionally classified: physics, industrial chemistry, catalysis, materials engineering, microelectronic materials, polymer science, biology, and geology.

The time is ripe for the broader chemical engineering community to be exposed to Car–Parrinello methods and their potential for chemical engineering. Computational methods, even very advanced ones, will continue to become more and more routine for nonspecialists. Having these computational methods in the chemical engineer's toolbox will necessarily lead to enhanced ability to make significant advances, both experimental and theoretical.

Moreover, chemical engineers think differently than scientists or other engineers, and this different way of thinking will lead to advances in Car–Parrinello methods that can be used in other fields. As chemical engineers, we always deal with inherently complex systems and have always focused on treating multiple scales, starting at the molecular level. Multiscale modeling, starting at the molecular scale and going to the macroscopic scale, is one of the current Grand Challenge Problems, spanning fields of science and engineering. Car-Parrinello methods present extremely powerful ways of treating the molecular scale and of scaling up to the macroscopic scale. Chemical engineers will help to solve the Grand Challenge Problem of multiscale modeling, and having methods such as Car–Parrinello methods in their toolbox is a prerequisite to solving them. Finally, many chemical engineers have asked me about recommended reviews on this subject. While many excellent reviews exist (see Appendix A), they do not address the field directly in a way that makes their potential readily evident to chemical engineers who are not already experts in these methods.

In this review, I have interpreted the term "Car–Parrinello methods" in the broad sense to mean those which combine first-principles quantum mechanical methods with molecular dynamics methods. I use this term synonymously with "*ab initio* molecular dynamics," "first-principles molecular dynamics," and "*ab initio* simulations." Thus, ways of solving the many-body electronic problem, such as Hartree–Fock and correlation methods, are included, in addition to the projector-augmented plane-wave method. In the original Car–Parrinello method, molecular motion is treated classically via

molecular dynamics and the wavefunction is propagated via fictitious electronic dynamics. I include methods based on this idea, in addition to other ways of keeping the wavefunction on the Born–Oppenheimer surface, such as optimization of the wavefunction at each molecular dynamics step. The latter method is often called "Born–Oppenheimer molecular dynamics."

I have designated "Car-Parrinello methods" in the plural for two main reasons. One is that, in deference to the impact of Car and Parrinello's classic 1985 paper, I am using this term to designate all ways of simulating the motion of atoms via combining a classical molecular dynamics treatment of the nuclei with a first-principles treatment of the electrons. The second, and perhaps most important, reason is that there are many molecular dynamics methods that have been and are being developed specifically for the simulation of atoms and molecules using forces calculated from derivatives of the quantum mechanical energy of these systems. It is the development of these methods that Car and Parrinello initiated.

## II. Objectives and Description of This Article

The objective of this article is to expose the chemical engineering community to Car–Parrinello methods, what they have accomplished, and what their potential is for chemical engineering. Consistent with this objective, in Section IV, I give an overview of the most widely used quantum mechanical method for solving the many-body electronic problem, density-functional theory, but describe other methods only cursorily. I also describe the practical solution of the equations of density-functional theory for molecular and extended systems via the plane-wave pseudopotential method, mentioning other methods only cursorily. Finally, I end this section with a description of the Car–Parrinello method itself.

In Section V, the longest one, I present a summary of the literature that presents methods and applications that tend to have the greatest relevance to chemical engineering, with an emphasis on work since 1997. I group the applications into several categories: gas-phase processes, processes in bulk materials, properties of liquids and processes in liquids, heterogeneous reactions and processes on surfaces, phase transitions, and processes in biological systems. In each category, I choose one or two case studies to pursue in detail and mention a few other relevant studies. Of course, there is an element of arbitrariness in choosing to focus on a few studies out of thousands, and certainly my exposure to the Parrinello group, both past and present, has made me more familiar with their work and more likely to choose applications from them. My hope is that chemical engineers will see how the methods

used in these applications can have relevance to their own areas of interest and will thus benefit from this review.

## III. Objectives of Car–Parrinello Methods and Classes of Problems to Which They Are Best Applicable

The reader can envision that the accurate calculation of the energy of a many-electron system is a computationally intensive endeavor, particularly when it must be performed thousands or tens of thousands of times, throughout a molecular dynamics trajectory. This section addresses the reasons one would wish to use these methods, in contrast to both experimental methods and molecular dynamics methods based on classical potentials. In its broadest sense, the reason for using Car–Parrinello methods is to determine properties of systems with as few fitted parameters or *a priori* assumptions as possible.

*Car–Parrinello methods contrasted with experimental approaches:* They can be used to study details of chemical systems that are difficult to address directly using experimental methods. One example is the nature and rate of elementary steps of catalytic processes. These are almost always very difficult to isolate experimentally.

*Car–Parrinello methods contrasted with classical molecular dynamic methods:* They can be used to obtain information about systems computationally, in which it is expected that conditions of the system change such that the range of validity of fitted potentials is exceeded. This is almost always the case when chemical bonds are broken and/or formed. It is also true for phase transitions or extreme states of high/low pressures and/or temperatures where not many experimental data exist. The accuracy of Car–Parrinello methods is not a strong function of the conditions to which they are applied (although they will be a function of the system to which they are applied).

*Car–Parrinello methods contrasted with static (0 K temperature) computational quantum mechanical methods:* They can treat entropy accurately without the need to use models such as the harmonic approximation for degrees of freedom of atomic motions. They can be used to sample potential energy surfaces on picosecond time scales, which is essential for treating liquids and aqueous systems. They can be used to sample reaction pathways or other chemical processes with a minimum of *a priori* assumptions. In addition, they can be used to find global minima [in conjunction with methods of optimization such as simulated annealing (Kirkpatrick *et al.,* 1983)] and to step out of local minima.

In summary, they are used both to understand trends in chemical systems as functions of composition, morphology, and thermodynamic conditions and to obtain information on the properties of specific chemical systems.

## IV. Methodology

Integral to Car–Parrinello methods is the use of computational quantum mechanics to determine the state of a number of electrons in the presence of any configuration of atomic nuclei. Determining the electronic state of the system quantum mechanically can be contrasted with using empirically derived potentials, such as Lennard–Jones or Morse potentials, used in classical methods. Once the electronic state has been computed, all properties of the system can be found. For molecular dynamics simulations, the most important properties are the absolute energy of the system and the forces on the individual atomic nuclei. Once these forces are computed, the nuclei can be propagated using classical equations of motion.

By far the major computational quantum mechanical method used to compute the electronic state in Car–Parrinello simulations is density-functional theory (DFT) (Hohenberg and Kohn, 1964; Kohn and Sham, 1965; Parr and Yang, 1989). It is the method used originally by Roberto Car and Michele Parrinello in 1985, and it provides the highest level of accuracy for the computational cost. For these reasons, in this section the only computational quantum mechanical method discussed is DFT. Section A consists of a brief review of classical molecular dynamics methods. Following this is a description of DFT in general (Section B) and then a description of practical DFT computations of chemical systems using the plane-wave pseudopotential method (Section C). The section ends with a description of the Car–Parrinello method and some basic issues involved in its use (Section D).

### A. Classical Molecular Dynamics

In classical molecular dynamics simulations, atoms are generally considered to be points which interact with other atoms by some predefined potential form. The forms of the potential can be, for example, Lennard–Jones potentials or Coulomb potentials. The atoms are given velocities in random directions with magnitudes selected from a Maxwell–Boltzman distribution, and then they are allowed to propagate via Newton's equations of motion according to a finite-difference approximation. See the following references for much more detailed discussions: Allen and Tildesley (1987) and Frenkel

and Smit (1996). To determine the magnitude and direction of motion of the nuclei at each time step, the force is computed on each nucleus by taking the negative of the gradient of the potential arising from the interaction of the atom with all other atoms in the simulation.

### B. Density-Functional Theory

To avoid using a predefined form for the interaction potential in molecular dynamics simulations, the quantum mechanical state of the many-electron system can be determined for a given nuclear configuration. From this quantum mechanical state, all properties of the system can be determined, in particular, the total electronic energy and the force on each of the nuclei. The quantum mechanically derived forces can then be used in place of the classically derived forces to propagate the atomic nuclei. This section describes the most widely used quantum mechanical method for computing these forces used in Car–Parrinello simulations.

Atomic nuclei are much heavier than electrons and can, in general, be treated accurately using a classical approach. Electrons, of course, must be treated quantum mechanically, and they are considered to move via the equations of quantum mechanics within the fixed external potential of the positively charged nuclei. Because of the relative speed of the motion of the electrons compared to that of the nuclei, their motion is, to an excellent approximation, separate from that of the nuclei in what is called the Born–Oppenheimer approximation. Moreover, excited electronic states are usually irrelevant at temperatures of interest to chemical engineers (<10,000 K), so only their ground state (minimum energy state) needs to be considered. (I do not consider here the interaction of radiation with matter, the treatment of which is not readily possible at this time using Car–Parrinello methods.)

One would then wish to solve the Schrödinger equation for the wavefunction of the electrons in the potential of the nuclei. This wavefunction would define the state of the system and can be used to obtain all observable properties of the system. The problem is that the many-body Schrödinger equation cannot be solved accurately, even using the most powerful of computers, except for the simplest of systems, consisting of only a few electrons.

Computational quantum mechanical methods, such as the Hartree–Fock method (Hehre *et al.,* 1986; Szabo and Ostlund, 1989; Levine, 2000), were developed to convert the many-body Schrödinger equation into a single-electron equation, which can then be solved tractably with modern computational power. The single-electron equation is an approach by which the state (or wavefunction) of each electron is computed within the field

of all of the other electrons. The major limitation of this approach is that electronic motion is correlated, and this electronic correlation cannot be treated exactly, except for very small systems. A tremendous amount of research has gone into treating electronic correlation (Szabo and Ostlund, 1989), and the general result is that one can consistently treat this correlation more and more accurately with a corresponding increase in computational cost.

An alternative to computing the properties of many-body electronic systems via the wavefunction is computing these properties via the electronic density. This approach was invented by Hohenberg and Kohn, who showed that the total energy of the many-body electronic system can be expressed as a functional of the density in the following way:

$$E[\rho(\mathbf{r})] = T[\rho(\mathbf{r})] + E_{\mathrm{e-e}}[\rho(\mathbf{r})] + E_{\mathrm{e-n}}[\rho(\mathbf{r})], \tag{1}$$

where $E[\rho(\mathbf{r})]$ is the total electronic energy, $T[\rho(\mathbf{r})]$ is the electronic kinetic energy, $E_{\mathrm{e-e}}[\rho(\mathbf{r})]$ is the contribution to the total energy from electron–electron interactions, and $E_{\mathrm{e-n}}[\rho(\mathbf{r})]$ is the contribution to the total energy from electron–nuclear interactions. (By convention, I have not written explicitly the nuclear–nuclear interaction, which is generally added directly to $E[\rho(\mathbf{r})]$ after the computation of $\rho(\mathbf{r})$ and $E[\rho(\mathbf{r})]$.)

The form of $E_{\mathrm{e-n}}[\rho(\mathbf{r})]$ is generally expressed as $\int \nu(\mathbf{r})\rho(\mathbf{r})\, d\mathbf{r}$, where $\nu(\mathbf{r})$ is the nuclear potential (*vide infra*), generally taken to be a Coulombic interaction. Finding accurate functional forms for $T[\rho(\mathbf{r})]$ and for $E_{\mathrm{e-e}}[\rho(\mathbf{r})]$ is a continuing challenge. In fact, a *major difference* between approaches based on the wavefunction and those based on the electronic density is that, in the latter case, accuracy cannot be systematically increased as it can in the former case.

To show the validity of using Eq. (1) to compute the total electronic energy of a many-electron system, Hohenberg and Kohn, in their famous 1964 paper, presented two proofs that provided the foundation for DFT. In the first, they proved that an external potential (such as classical nuclei distributed in space) is a unique functional of the electron density (apart from a trivial additive constant). For most practical purposes, the converse is true, and the electron density of $N$ electrons in an external potential is considered to result uniquely from that potential. Parr and Yang (1989) give an in-depth discussion of these issues, in addition to providing the staple text on DFT. We also remind the reader that a functional maps a set of functions to a set of numbers, in contrast to a function, which maps one set of numbers to another set of numbers.

In the second proof, Hohenberg and Kohn showed that there exists a universal functional of the electronic density, $F[\rho(\mathbf{r})]$, independent of the

external potential, $v(\mathbf{r})$, such that the energy of the system,

$$E \equiv \int v(\mathbf{r})\rho(\mathbf{r})\, d\mathbf{r} + F[\rho(\mathbf{r})], \tag{2}$$

has its minimum at the correct ground-state energy. For the systems of interest here,

$$v(\mathbf{r}) = \sum_{I}^{N_I} \frac{1}{|\mathbf{R}_I - \mathbf{r}|}, \tag{3}$$

where $N_I$ is the number of atomic nuclei (ions) and $\mathbf{R}_I$ is the position of each nucleus.

The consequences of what Hohenberg and Kohn showed are that if $F[\rho(\mathbf{r})]$ can be found, the unique ground-state electronic density can be found for any configuration of nuclei [i.e., external potential $v(\mathbf{r})$], and this ground-state electronic density can then be used in place of the wavefunction to define the electronic state of the system and, thus, all observable properties of the system.

$F[\rho(\mathbf{r})]$ can be divided into a contribution from the kinetic energy of the electrons, $T[\rho(\mathbf{r})]$, and the energy of interaction of all of the electrons, $E_{\mathrm{e-e}}[\rho(\mathbf{r})]$:

$$F[\rho(\mathbf{r})] = T[\rho(\mathbf{r})] + E_{\mathrm{e-e}}[\rho(\mathbf{r})]. \tag{4}$$

$E_{\mathrm{e-e}}[\rho(\mathbf{r})]$ can be further divided into three terms:

$$E_{\mathrm{e-e}}[\rho(\mathbf{r})] = J[\rho(\mathbf{r})] + E_{\mathrm{x}}[\rho(\mathbf{r})] + E_{\mathrm{c}}[\rho(\mathbf{r})], \tag{5}$$

where $J[\rho(\mathbf{r})]$ is the mean-field electronic interaction term, traditionally designated with the symbol $J$, from Hartree–Fock theory,

$$J[\rho(\mathbf{r})] = \iint \frac{\rho(\mathbf{r})\rho(\mathbf{r}')}{|\mathbf{r} - \mathbf{r}'|} d\mathbf{r}\, d\mathbf{r}'. \tag{6}$$

$E_{\mathrm{x}}[\rho(\mathbf{r})]$ is the correction due to Pauli exchange (correlation between electrons of the same spin), and $E_{\mathrm{c}}[\rho(\mathbf{r})]$ is the correction due to all other electronic correlations (primarily between electrons of differing spins). We note that, here and below, all quantities are expressed as atomic units (Hehre *et al.,* 1986), so that no conversion constants need to be included in the equations. Also, as stated above, the nuclear–nuclear repulsion can be added trivially and is considered implicit in the equations presented.

There are two major issues involved in applying the formalism described above. (i) There exists no good functional for the electronic kinetic energy, $T[\rho(\mathbf{r})]$, and (ii) there exists no exact expression for $E_{\mathrm{x}}[\rho(\mathbf{r})]$ or for $E_{\mathrm{c}}[\rho(\mathbf{r})]$. Issue ii has been addressed by the continuing development of more and more accurate functionals for $E_{\mathrm{x}}[\rho(\mathbf{r})]$ and for $E_{\mathrm{c}}[\rho(\mathbf{r})]$. A bit more detail on these functionals is described below. Issue i is drastic and was overcome by Kohn

and Sham (1965) in a way that allows the computation of almost the exact electronic kinetic energy, but with a dramatic increase in the computational cost of a density functional theory calculation.

Kohn and Sham's approach is to replace the kinetic energy functional with the exact kinetic energy functional for a noninteracting reference state and then to incorporate into $E_c[\rho(\mathbf{r})]$ the correction in the kinetic energy between the noninteracting reference state and the interacting state. The kinetic energy of the noninteraction reference state is expressed as

$$T_s[\rho(\mathbf{r})] = \sum_i^N \int \psi_i^*(\mathbf{r}) \left(-\frac{1}{2}\nabla^2\right) \psi_i(\mathbf{r})\, d\mathbf{r}, \tag{7}$$

where the $\psi_i(\mathbf{r})$'s are the one-electron (orthonormal) Kohn–Sham orbital wavefunctions. Recall that

$$\rho(\mathbf{r}) = \sum_i^N |\psi_i(\mathbf{r})|^2. \tag{8}$$

(We note that, here and below, we have developed the formalism for spin-paired systems, e.g., systems for which the net spin is zero. It is straightforward to generalize this formalism to treat systems with nonzero spin.)

Now the total energy of the many-electron system can be expressed as

$$E[\rho(\mathbf{r})] = T_s[\rho(\mathbf{r})] + \int v(\mathbf{r})\rho(\mathbf{r})\, d\mathbf{r} + J[\rho(\mathbf{r})] + E_{xc}[\rho(\mathbf{r})], \tag{9}$$

where

$$E_{xc}[\rho(\mathbf{r})] = T[\rho(\mathbf{r})] - T_s[\rho(\mathbf{r})] + E_x[\rho(\mathbf{r})] + E_c[\rho(\mathbf{r})]. \tag{10}$$

The ground state $\rho(\mathbf{r})$ which is the solution to Eq. (9) is then that which minimizes $E[\rho(\mathbf{r})]$, subject to the constraint that the one-electron orbital wavefunctions, $\psi_i$'s, which constitute $\rho(\mathbf{r})$ as expressed in Eq. (8), are orthonormal:

$$\int \psi_i^*(\mathbf{r})\psi_j(\mathbf{r})\, d\mathbf{r} = \delta_{ij}, \tag{11}$$

where $\delta_{ij}$ is the Krönicker $\delta$ function.

Combining Eqs. (7) and (8) with Eq. (9) yields an expression for the total energy as a functional of the Kohn–Sham orbitals. This expression can be solved subject to the constraints in Eq. (11) using the method of Lagrange's undetermined multipliers. We can write

$$\mathcal{L} = E[\rho(\mathbf{r}) - \sum_i^N \sum_j^N \varepsilon_{ij} \int \psi_i^*(\mathbf{r})\psi_j(\mathbf{r})\, d\mathbf{r}, \tag{12}$$

where the $\varepsilon_{ij}$'s are the Lagrange multipliers.

$\mathcal{L}$ is then functionally minimized with respect to each $\psi_i$, yielding $N$ coupled Euler–Lagrange equations of the form

$$\left[-\frac{1}{2}\nabla^2 + v_{eff}(\mathbf{r})\right]\psi_i(\mathbf{r}) = \varepsilon_i\psi_i(\mathbf{r}), \qquad i = 1, 2, 3, \ldots, N, \tag{13}$$

where

$$v_{eff}(\mathbf{r}) = v(\mathbf{r}) + \int \frac{\rho(\mathbf{r}')}{|\mathbf{r} - \mathbf{r}'|}d\mathbf{r}' + v_{xc}(\mathbf{r}), \tag{14}$$

and

$$v_{xc}(\mathbf{r}) = \frac{\delta E_{xc}[\rho(\mathbf{r})]}{\delta\rho(\mathbf{r})} \tag{15}$$

the functional derivative of $E_{xc}[\rho(\mathbf{r})]$.

All that remains is to choose a functional form for $E_{xc}[\rho(\mathbf{r})]$. There are quite a number that have proposed and tested, and developing more and more accurate exchange-correlation functionals is an area of ongoing research. The functionals are usually labeled by the agglomeration of the initials of the surnames of the inventors. Typical examples are BLYP (Becke, 1988; Lee *et al.,* 1988), PW (Perdew and Wang, 1992), PBE (Perdew *et al.,* 1996), and HCTH/120 (Boese *et al.,* 2000). These are all universal functionals with fitted parameters that are fixed and used for any system. There is little known on how to choose a given functional for a particular problem to maximize accuracy, although extensive studies on the heats of formation of gas-phase molecules have been performed by Curtiss *et al.* (1997). Often several functionals are tested for a particular system, and the one that best matches experimental results is chosen. Othertimes, a particular functional is chosen and then its accuracy for calculating the properties of a particular system is determined by comparison to related experimental results. As a rule of thumb, bond energies computed using these functionals have an error of ~5 kcal/mol, and bond lengths and angles have an error of ~1% compared to experiment. It is strongly advised, however, to compare whatever experimental data are available to the computed result for the particular system studied.

### C. Choice of Model and Solution of the Equations Using Plane-Wave Basis Sets and the Pseudopotential Method

Once the exchange-correlation functional is chosen, the $N$ one-electron coupled, nonlinear Eqs. (13) can be solved self-consistently for the $\psi_i$'s. To

do this, a suitable expansion is chosen for the $\psi_i$'s. This expansion is called a "basis set." (Note that the term "basis set" used in this context differs from that which mathematicians would term a basis set.)

The form of the basis set expansion is chosen to be convenient to model the system and to perform the integrals needed to solve the coupled Eqs. (13). Examples of convenient forms are Gaussians, numerical grids, and plane waves. Plane waves have often (but not exclusively) been chosen as the basis set expansion used in Car–Parrinello simulations for two reasons: (i) It is generally desired to simulate extended systems, such as bulk materials, surfaces, and liquids, and plane waves provide a convenient way to model these systems using periodic boundary conditions; (ii) forces on atomic nuclei can be calculated very efficiently if the electrons are described by plane waves by making use of the Hellman–Feynman theorem (*vide infra*).

Typically the model chosen is a collection of nuclei with corresponding electrons in a periodically repeated cell, called a "supercell." This supercell can have any space filling symmetry. If the system is a crystal, having translational symmetry, the supercell may have one or more unit cells. If the system is an amorphous solid or a liquid, a large enough supercell must be chosen so that correlations introduced by the periodic symmetry do not affect greatly the properties to be determined in the calculation. Finally, if the system is a surface, generally a "slab model," several atomic layers thick, is chosen and enough vacuum space is left so that spurious periodic interactions to not occur. Generally 5–6 Å of vacuum is enough. Examples of supercells with repeated images for each of these three cases are presented in Figs. 1–3.

Plane waves have the following form:

$$f_i = \frac{1}{\sqrt{\Omega}} e^{i\mathbf{g}\cdot\mathbf{r}}, \tag{16}$$

where $\Omega$ is the volume of the cell, and $\mathbf{g}$ is a reciprocal lattice vector of the cell. The $\psi_i$'s in Eqs. (11)–(13) cannot, however, simply be expressed as a summation of $f_i$'s over reciprocal lattice vectors, because application of the Bloch theorem to electronic orbitals in periodic potentials leads to the introduction of wave vectors, $\mathbf{k}$, lying in the first Brillouin zone (see, e.g., Ashcroft and Mermin, 1976).

Thus, using periodic boundary conditions, the $\psi_i$'s, in Eqs. (11)–(13) are expanded at each wave vector $\mathbf{k}$ (also stated "at each k-point") in terms of plane waves as follows:

$$\psi_i^{\mathbf{k}} = \sum_{\mathbf{g}} c_i^{\mathbf{k}}(\mathbf{g}) e^{i(\mathbf{g}+\mathbf{k})\cdot\mathbf{r}}, \tag{17}$$

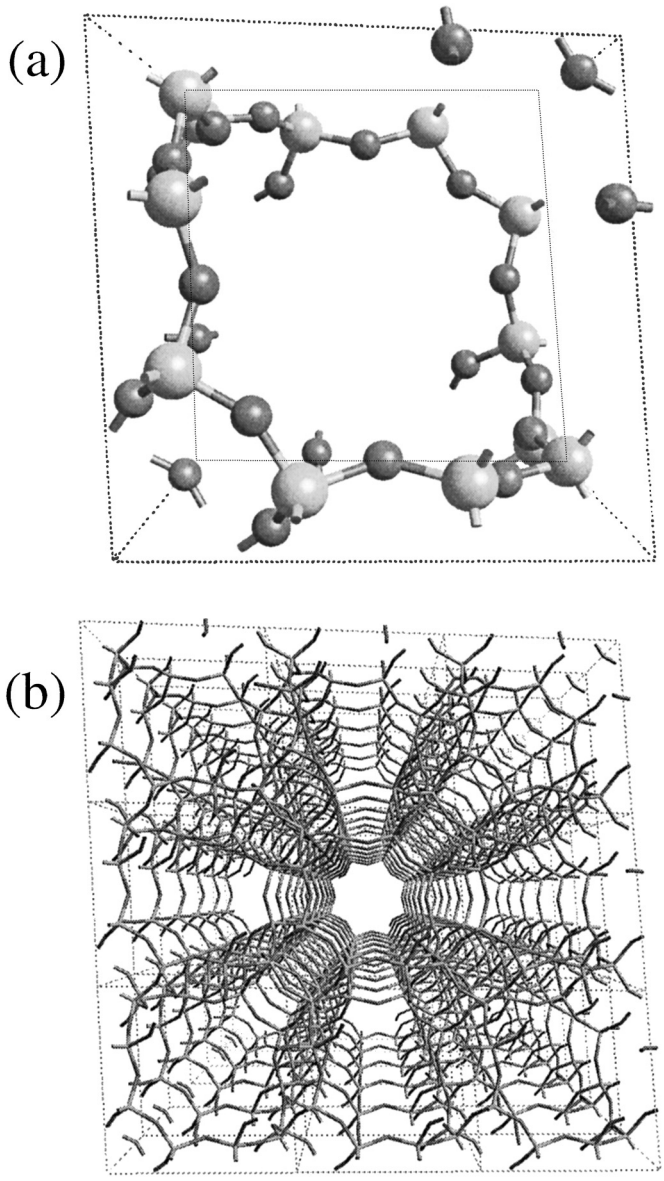


FIG. 1. (a) A trigonal unit cell of the zeolite chabazite, consisting of 36 atoms. This unit cell is also chosen as the supercell. (b) A perspective view down a channel of chabazite; 54 unit cells are displayed.

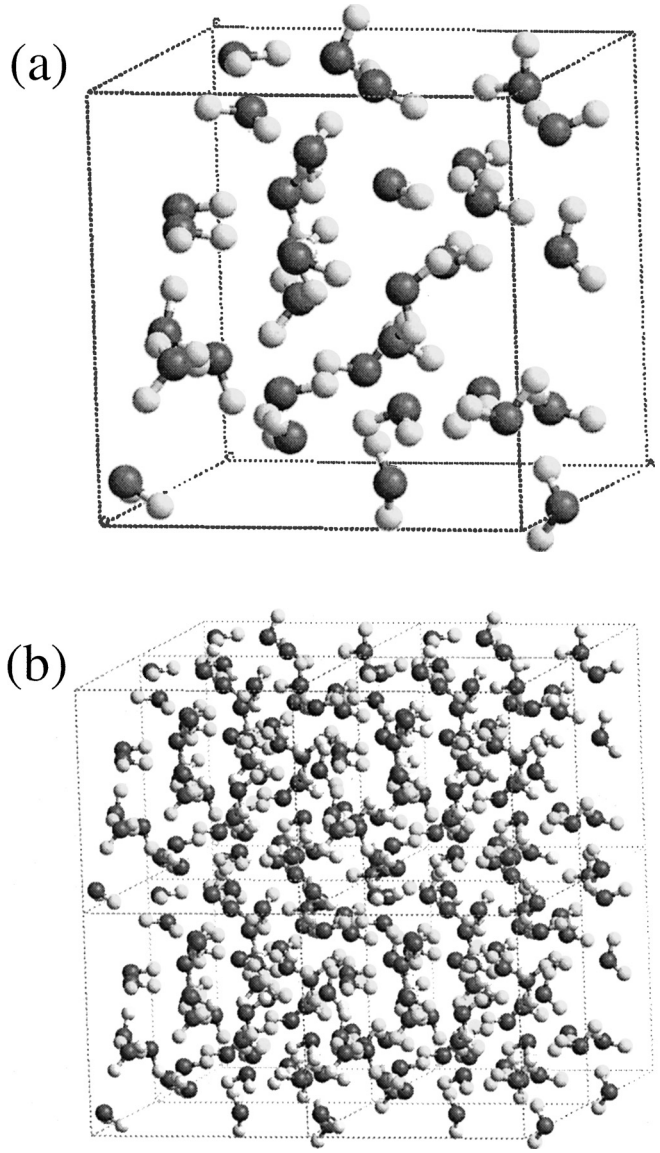


FIG. 2. (a) A cubic supercell containing 32 water molecules. The cell is chosen so that the density is 1.00 g/cm$^3$. (b) Eight supercells demonstrating the disorder of the system.

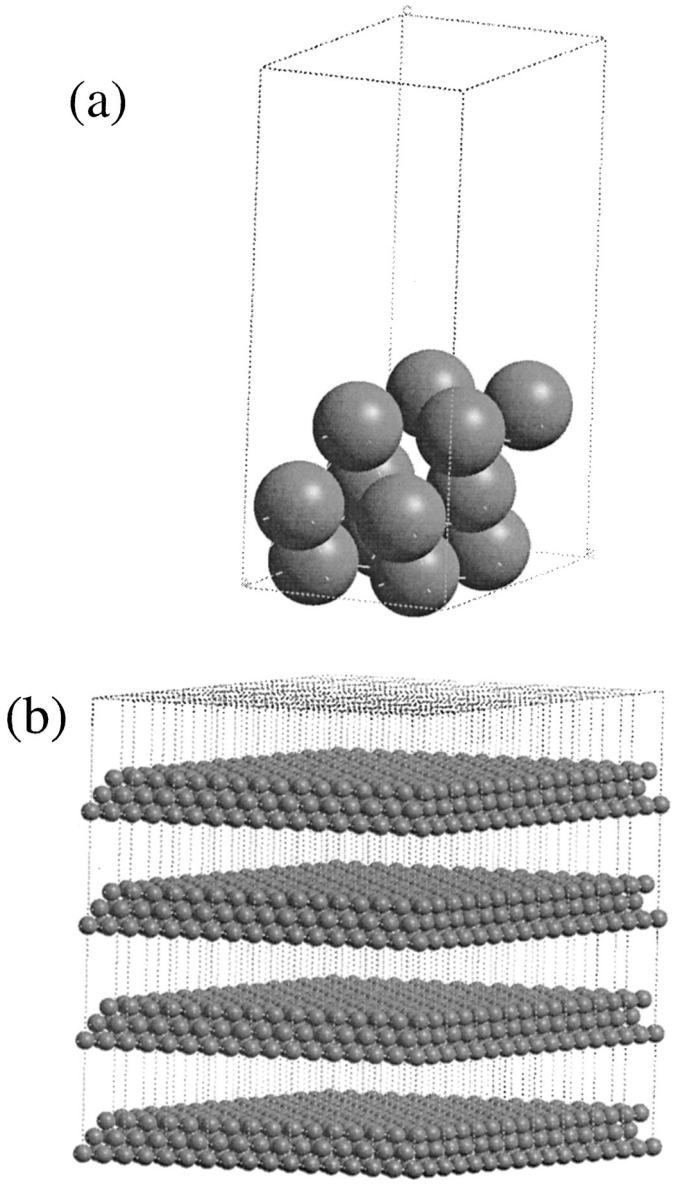


FIG. 3. (a) A slab model of the platinum (111) surface, consisting of 12 atoms. The symmetry of the supercell is hexagonal. (b) Two hundred fifty-six supercells.

where the $c_i^{\mathbf{k}}(\mathbf{g})$'s are coefficients to be determined in the calculation. Now the $\psi_i$'s in Eqs. (6)–(12) must be replaced by $\psi_i^{(\mathbf{k})}$'s and the electron density [Eq. (7)] becomes

$$\rho(\mathbf{r}) = \sum_{\mathbf{k}} w_{\mathbf{k}} \sum_i y_i^{\mathbf{k}} \left|\psi_i^{\mathbf{k}}\right|^2, \tag{18}$$

where $w_{\mathbf{k}}$ is the weight of each k-point, and $y_i^{\mathbf{k}}$ is the occupation number of each orbital $i$ at each k-point. For these expansions to be exact, the summations over $\mathbf{k}$ and $\mathbf{g}$ should be infinite. In practice, the number of k-points in the summation can often be small, since sets of special k-points can be chosen for a given lattice symmetry. The summation over $\mathbf{g}$ is then performed to include all of those reciprocal lattice vectors with energy $E = \frac{1}{2}(\mathbf{k}+\mathbf{g})^2$ less than a cutoff energy, $E_{\text{cut}}$. $E_{\text{cut}}$ is generally expressed in units of Rydbergs and is generally roughly between 10 and 100 Ry. For a 1-nm$^3$ cell this corresponds to 10,000 to 100,000 plane waves per k-point for each Kohn–Sham orbital.

Plane waves, while natural for describing electronic orbitals in periodic potentials, do not describe the orbitals well near the nuclei, where electronic gradients can be quite large. In fact, to describe properly these orbitals near the nuclei, expansions much larger than those mentioned above would have to be used, unless a special technique were used to treat the core electronic region. This technique is called the "pseudopotential method." In this method, the core electrons are replaced with a fixed potential (which is generally nonlocal), and only the valence electrons are treated explicitly. Such an approach is validated by the fact that, in general, the energy levels of core electrons do not change under different chemical environments as evidenced by numerous XPS data. When plane waves are the chosen basis functions and pseudopotentials are used, this method is called the "plane-wave pseudopotential method."

Using pseudopotentials has several major beneficial consequences: (i) Only the valence electrons must be treated explicitly, thus the number of equations to be solved [Eqs. (13)] can be reduced drastically; (ii) the pseudo-orbitals are very smooth near the atomic core, and thus $E_{\text{cut}}$ can be reduced drastically; and (iii) important relativistic effects of the core electrons of heavy elements such as the 5d elements can be included in nonrelativistic calculations. The major downsides are that the potential $v(\mathbf{r})$ in Eq. (3) must be replaced with a more complicated and computationally expensive nonlocal pseudopotential and, more importantly, that the transferability of the pseudopotential, i.e., its accuracy in different bonding environments, may not be perfect. Developing highly transferable pseudopotentials that can be used at as low an $E_{\text{cut}}$ as possible is a major current topic of research.

Once the k-points and the basis set expansion for the $\psi_i^{\mathbf{k}}$'s are chosen, the coupled Eqs. (13) can be solved self-consistently for the coefficients, $c_i^{\mathbf{k}}(\mathbf{g})$. The total electronic energy of the system can then be calculated via

Eq. (9), and the forces on the nuclei can also be determined. More details on pseudopotential methods, on methods of solving the Kohn–Sham equations, and on the algorithms used can be found in the references described in Appendix A.

As noted above, when the orbitals are expanded in terms of plane waves, forces can be calculated accurately and efficiently using the Hellman–Feynman theorem. This theorem states that the sum of the last two terms of the derivative of the total energy with respect to a nuclear coordinate $\lambda$, expressed in Dirac notation as follows,

$$\frac{d}{d\lambda}E(\lambda) = \langle\psi(\lambda)|\frac{d}{d\lambda}H(\lambda)|\psi(\lambda)\rangle + \left[\frac{d}{d\lambda}\langle\psi(\lambda)|\right]H(\lambda)|\psi(\lambda)\rangle + \langle\psi(\lambda)|H(\lambda)\left[\frac{d}{d\lambda}|\psi(\lambda)\rangle\right] \tag{19}$$

are equal to zero. Thus,

$$\frac{d}{d\lambda}E(\lambda) = \langle\psi(\lambda)|\frac{d}{d\lambda}H(\lambda)|\psi(\lambda)\rangle. \tag{20}$$

This theorem is, of course, valid only when $\psi$ is described exactly. Because plane waves describe all of space evenly and are not centered on atomic nuclei, Eq. (20) can be used to calculate forces accurately for approximate plane-wave expansions of $\psi$. For expansions of $\psi$ in terms of atomic centered basis functions such as Gaussians and atomic centered grids, Eq. (19) must be used. This is because space is not covered uniformly by atomic centered basis functions, and thus, errors in $\psi$ are nonuniform, and the last two terms in Eq. (19) do not add to zero. The added expense of calculating forces via Eq. (19) often prohibits the use of atomic centered basis functions in molecular dynamics simulations.

### D. Car–Parrinello Molecular Dynamics

The forces on each atomic nucleus, calculated quantum mechanically for a given nuclear configuration, can then be used in one of the finite-difference methods for propagating the atomic nuclei described in Section A above. One might envision solving for the orbitals and forces for a given nuclear configuration as described in Section B, advancing the nuclear positions in time, computing the orbitals and forces for the new nuclear configuration, etc. This method, called "Born–Oppenheimer molecular dynamics" is currently used by many researchers, but it is different from the original method developed by Car and Parrinello, which is also the primary method used today.

The Car–Parrinello method presents a trick to propagate the orbitals along with the nuclei without reoptimizing them at each molecular dynamics step. It does so by introducing a fictitious orbital mass and propagating the orbitals *with* the nuclei via appropriate equations of motion. The Car–Parrinello Lagrangian is

$$L = \sum_i \frac{1}{2} \int d\mathbf{r} \mu |\dot{\psi}_i(\mathbf{r})|^2 + \sum_i \frac{1}{2} M_I \dot{R}_I^2 - E[\{\psi_i(\mathbf{r})\}, R_I] + \sum_{ij} \Lambda_{ij} \left( \int d\mathbf{r} \psi_i^*(\mathbf{r}) \psi_j(\mathbf{r}) - \delta_{ij} \right). \tag{21}$$

(Note that for simplicity, I have not written explicitly the k-point indices or the orbital occupancies.) In Eq. (21), the second term is the kinetic energy of the nuclei and the third term is the potential energy of the nuclei, which is also the electronic energy [Eq. (9) if calculated via DFT]. The first term is the fictitious kinetic energy of the orbitals, where $\mu$ is the fictitious mass of the orbitals. The fourth term is a set of constraints which keep the orbitals orthonormal, where $\Lambda_{ij}$ are the undetermined multipliers. Note that additional constraints can be added into this Lagrangian (*vide infra*).

From this Lagrangian, the following equations of motion are generated:

$$\mu \ddot{\psi}_i(\mathbf{r}, t) = -\frac{\delta E[\{\psi_i(\mathbf{r}, t)\}, R_I]}{\delta \psi_i^*(\mathbf{r}, t)} + \sum_j \Lambda_{ij} \psi_j(\mathbf{r}, t) \tag{22a}$$

$$M_I \ddot{R}_I = -\nabla_{R_I} E[\{\psi_i(\mathbf{r}, t)\}, R_I]. \tag{22b}$$

Thus, the orbitals are propagated with the nuclei, although while the nuclear motion is physical, the motion of the orbitals is only a means to adjust the orbitals so that they remain on the ground-state (Born–Oppenheimer) surface. The original idea of Car and Parrinello was to use these equations of motion to optimize simultaneously the orbitals and the nuclear configuration, using a method of dynamic simulated annealing (Kirkpatrick *et al.,* 1983). As it turns out, Car–Parrinello calculations are rarely performed to do exactly this, although they are often used to find structural properties of materials by allowing the nuclei to jump over small barriers. Their primary power, however, comes in their ability to investigate the short-time dynamics of systems and to sample reaction pathways within various ensembles.

We might ask why this method works and, even more importantly from a practical standpoint, when it will not work. The motion of the orbitals for

small deviations from the ground state can be described by a superposition of oscillations with frequencies:

$$\omega_{ik} = \left(\frac{2(\varepsilon_k - \varepsilon_i)}{\mu}\right)^{\frac{1}{2}}, \tag{23}$$

where $\varepsilon_k$ is the eigenvalue of an unoccupied state and $\varepsilon_i$ is the eigenvalue of an occupied state. Thus, the lowest orbital frequency is $\omega_{\min} = (2E_g/\mu)^{\frac{1}{2}}$, where $E_g$ is the energy gap (HOMO–LUMO gap for molecules). Choosing a typical value of $\mu$ of 400 a.u. and for typical values of $E_g$ of $\sim$2 eV, $\omega_{\min}$ is of the order of 1000 THz, versus the highest frequency of the nuclear motion of about 100–200 THz (Galli and Parrinello, 1991). This separation in the rate of orbital and nuclear motion allows the orbitals to follow the motion of the nuclei, while remaining on their ground-state (Born–Oppenheimer) surface. The values of $\mu$ and $M_I$ are major factors in determining the minimum time step necessary for accurate integration in the molecular dynamics simulation. A typical value of the time step in a Car–Parrinello simulation for the situation described above is $\sim$0.1 fs.

As $E_g$ gets smaller, $\mu$ must be set smaller, and consequently, the molecular dynamics time step must be set smaller. If the time step is too large, there will be an exchange of energy between the nuclear and the orbital motion, and the orbitals will not remain on the ground-state (Born–Oppenheimer) surface. When this occurs, the effect on the simulation is disastrous. Obviously, the smaller the molecular dynamics time step is, the less efficient the simulation is. This will be a problem for metals in particular, where $E_g$ will be very small (0 for an infinite system). There are two ways of addressing this problem. One is by attaching a thermostat to control the motion of the orbitals (Galli and Parrinello, 1991), and the other is by performing Born–Oppenheimer molecular dynamics as described at the beginning of Section D.

I close this section by noting that the choice of performing Car–Parrinello molecular dynamics, using Eqs. (22a) and (22b) versus Born–Oppenheimer molecular dynamics should be made as a trade-off between efficiency and accuracy. There have been only a few studies on this choice, an excellent description of which is given by Marx (2000).

## V. Applications

The methodology described above provides the ability to perform molecular dynamics simulations without choosing forms and parameters for interaction potentials. Because Car–Parrinello simulations are molecular

dynamics simulations, all methodologies developed for classical molecular dynamics simulations can be used in Car–Parrinello methods. Thus, $(N,V,T)$ simulations can be performed in addition to $(N,P,T)$ simulations, etc. When the interaction among atoms is determined quantum mechanically, the breaking and formation of bonds can be treated accurately, and charge distributions, polarizability, and charge transfer, in addition to other properties, can be computed.

The downside to the power of Car–Parrinello calculations is that they are computationally costly. Typically, the largest systems that can be treated are of the order of 100 atoms, and the time scale of the simulations is of the order of picoseconds. The purposes of Car–Parrinello simulations generally fall under three main categories: (i) simulations as a means of optimization to determine structural properties, (ii) direct simulations of processes occurring over short time scales, and (iii) simulations to sample equilibrium properties.

The majority of Car–Parrinello simulations performed so far fall under category i. Car–Parrinello simulations allow nuclei to hop over small energetic barriers, whereas typical geometry optimizations (with dynamics) yield only the closest local minimum to the starting point. Examples falling under this category include the calculation of elastic constants, interfacial structures of electronic materials and grain boundaries, molecular crystals, minerals, and structures of various defects. Two notable examples are given by Haase *et al.* (1997) and by Janotti *et al.* (1997) and Papoulias *et al.* (1997).

Haase *et al.* (1997) studied methanol adsorption at active sites of an acidic chabazite catalyst (see Fig. 1). They addressed a long-standing controversy of whether methanol is chemisorbed at the acid site (the acidic proton is transferred to the methanol) or physisorbed (the acidic proton is not transferred to the methanol). Previous quantum mechanical studies were inconclusive, primarily because the highly corrugated potential energy surface had many local minima in the region of interest, and this surface was very difficult to sample comprehensively. By allowing the entire system to move dynamically at 400 K, Haase *et al.* (1997) were able to sample a range of local minima and showed that the lowest energy of adsorption of methanol was the physisorbed state.

Both Janotti *et al.* (1997) and Papoulias *et al.* (1997) studied the formation of defects in GaAs. Using Car–Parrinello methods to optimize simultaneously the orbitals and the geometry of their system, Janotti *et al.* (1997) predicted the stability of various defect pairs over others, in addition to the properties of those defect pairs. Papoulias *et al.* (1997) studied As interstitial pairs in As-rich GaAs. Previous static studies had shown that there are many different defect pairs possible with stable minima. Papoulias *et al.* (1997) showed that the lowest energy defect consisted of As atoms forming a pair of split interstitials centered on nearest-neighbor sites. They also

investigated the electronic properties of these As pairs and concluded that they are electrically inactive, thus explaining experimental observations of a large number of inactive As in GaAs grown using certain methods.

Studies under categories ii and iii provide more poignant examples of the power of Car–Parrinello methods. Because of the magnitude of the literature on applications of Car–Parrinello simulations, I have chosen to focus on a few case studies to illustrate the potential of simulations under these categories for problems of interest to chemical engineers. The areas that I have chosen are (A) gas-phase processes; (B) processes in bulk materials; (C) properties of liquids, solvation, and reactions in liquids; (D) heterogeneous reactions and processes on surfaces; (E) phase transitions; and (F) processes in biological systems.

## A. Gas-Phase Processes

Gas-phase systems, if they are small enough, are convenient to study, because of the relatively small computational time. To study such systems using the plane-wave pseudopotential method, large supercells must be chosen to avoid spurious interactions from periodic potentials. Of course, if localized basis functions are chosen, such as Gaussians, there is no periodicity.

Two example studies used Car–Parrinello methods to study gas-phase reactions directly. These fall under category ii described above. Yamataka *et al.* (1999) simulated the reaction of the formaldehyde radical anion and methyl chloride. Frank *et al.* (1998) simulated the reaction of OH radicals with ketones.

Since the reaction of the formaldehyde radical anion with methyl chloride involves overcoming a barrier over time scales much larger than a picosecond, Yamataka *et al.* (1999) could not directly simulate the entire reaction process. Instead, they started at a transition-state structure, known from static quantum mechanical calculations; chose random initial velocities; and performed nine simulations at 298 K. Three of these simulations resulted in the formation of the reactants, three resulted in the formation of products via an electron-transfer reaction, and three resulted in the formation of products via a carbon-substituted $S_N2$ reaction. These three sets of resulting structures are shown in Fig. 4.

The trajectories of the electron-transfer process consisted of three phases as shown in Fig. 5. During the first phase, up to about 30 fs, there was not much change. During the second phase, which occurred over the next 200 fs, the chlorine atom starts separating from its adjacent carbon atom, but after an initial drop, the total energy remains constant. After this period, during phase 3, the carbon–carbon distance increases, and both the charge and the

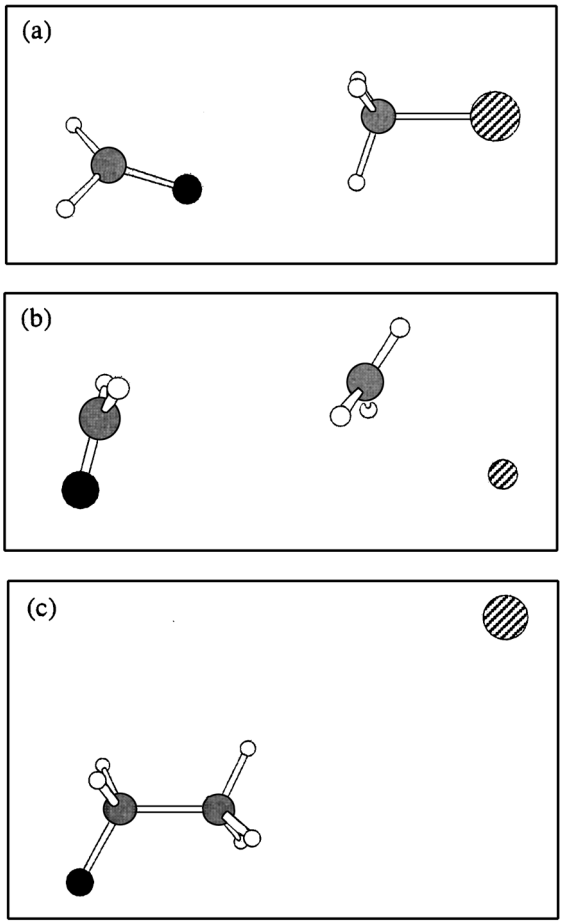


FIG. 4. Snapshots of structures obtained (a) after 500 fs in a trajectory leading to the reactant state, (b) after 300 fs in a trajectory leading to the electron-transfer product, and (c) after 300 fs in a trajectory leading to the $S_N2$ products. Reprinted with permission from Yamataka *et al.* (1999).

spin density on each species stabilize. The simulations by Yamataka *et al.* (1999) support the notion that products could be formed either via an $S_N2$ process or via an electron-transfer process at 298 K. They also produced a detailed analysis of the nature of the reaction process.

Ketones are organic pollutants which react with OH in the atmosphere. As an alternative to performing expensive and time-consuming experimental studies on these reactions, Frank *et al.* (1998) chose to evaluate the reactivity

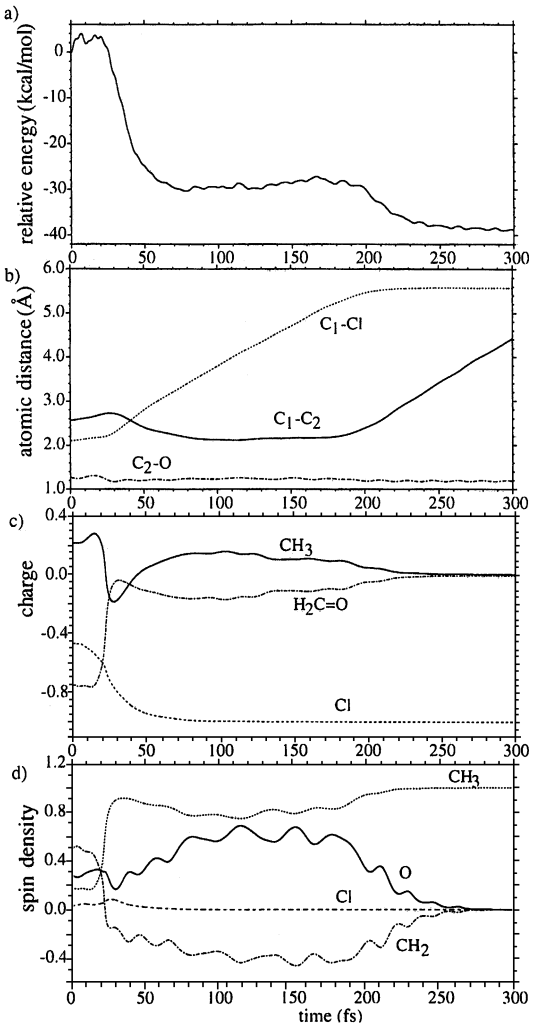


FIG. 5. Sample trajectory leading to the electron-transfer product. (a) Electronic energy, (b) atomic distances, (c) Mulliken group charges, and (d) spin density. Reprinted with permission from Yamataka *et al.* (1999).

of various ketones with OH using Car–Parrinello simulations. As in the previous example, reaction barriers prevent simulating an entire reaction process at ambient temperatures. Thus, to evaluate relative reactivities of various ketones, Frank *et al.* (1998) chose initial reactant configurations and gave the species relatively high kinetic energies with velocities sampled from Maxwell–Boltzman distributions. In this way, they were able to delineate two

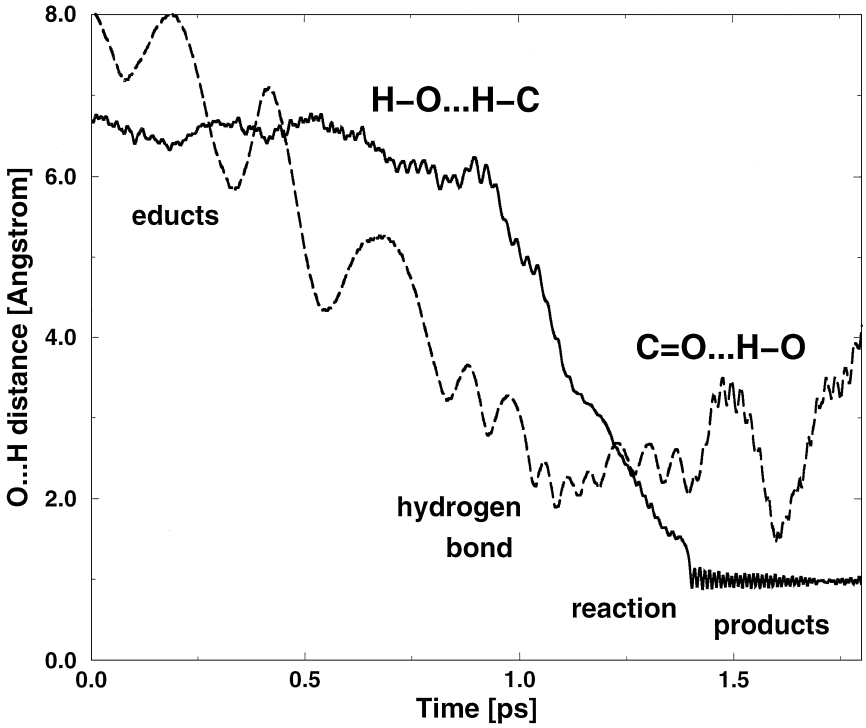


FIG. 6. The low-energy reaction process of an OH radical with a ketone. The solid line shows, as a function of time, the distance between the oxygen atom in the OH radical and the hydrogen atom in the ketone molecule. The dashed line shows, as a function of time, the distance between the oxygen atom in the ketone molecule and the hydrogen atom in the OH radical. Reprinted with permission from Frank *et al.* (1998).

reaction mechanisms for the process, depending on the kinetic energy. This implies that the product distribution will be a strong function of the kinetic energy of the reactants.

The mechanism at high kinetic energies was a simple abstraction process. At lower kinetic energies, a more complex mechanism ensues, as illustrated in Figs. 6 and 7. Initially, a hydrogen bridge is formed. Next, the oxygen atom in the OH approaches one of the hydrogen atoms in the ketone, leading to a ring structure. Finally, the hydrogen bridge is broken, leading to a free water molecule and a ketyl radical. It should be noted that the ring structure (Fig. 7, bottom left) does not correspond to a local minimum and would not have been observed by static quantum calculations.

Other gas-phase studies include the thermal dissociation of acetic acid (Liu *et al.,* 1999b), and the study of the reaction $Cl^- + CH_3Br \rightarrow CH_3Cl + Br^-$

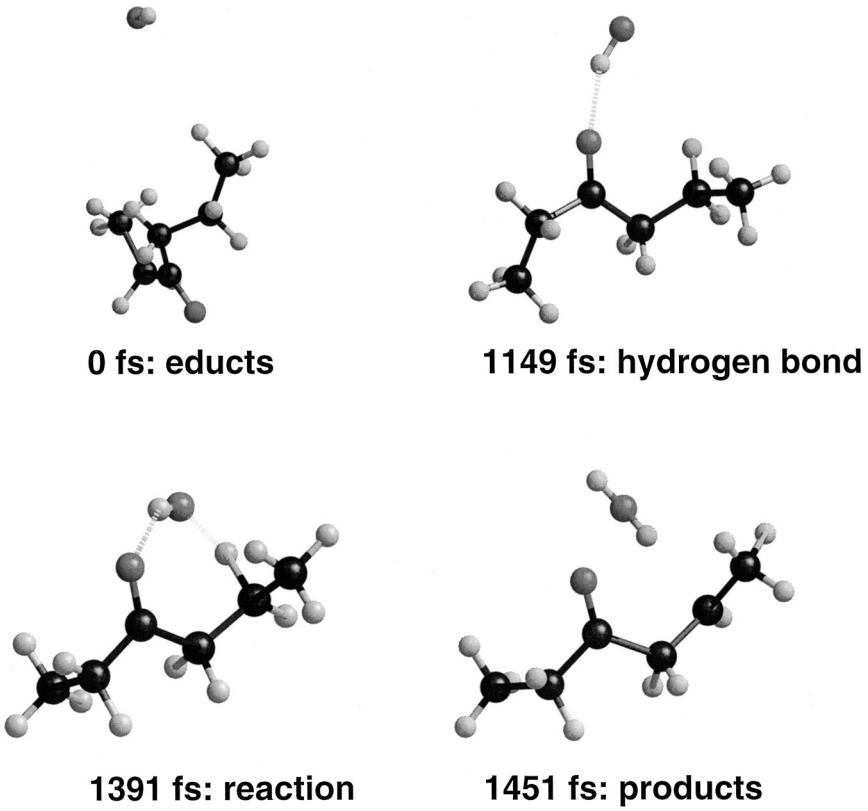


FIG. 7. Snapshots of the low-energy reaction process of an OH radical with a ketone. Reprinted with permission from Frank *et al.* (1998).

(Raugei *et al.,* 1999). There have also been quite a number of studies on gas-phase clusters of varying types, in addition to several other gas-phase reactions, including isomerization reactions.

## B. PROCESSES IN BULK MATERIALS

Aside from using Car–Parrinello methods to evaluate structural properties and relaxation processes in bulk materials, they have been used under category ii to evaluate directly diffusivities of ions in materials. Wengert *et al.* (1996) studied the diffusivities of Si, Mg, and Li in the superionic conductor, $Li_{2-2x}Mg_{1+x}Si$ ($x \sim 0.06$) at 600, 900, and 1400 K. Some of their results from their trajectories are presented in Fig. 8.

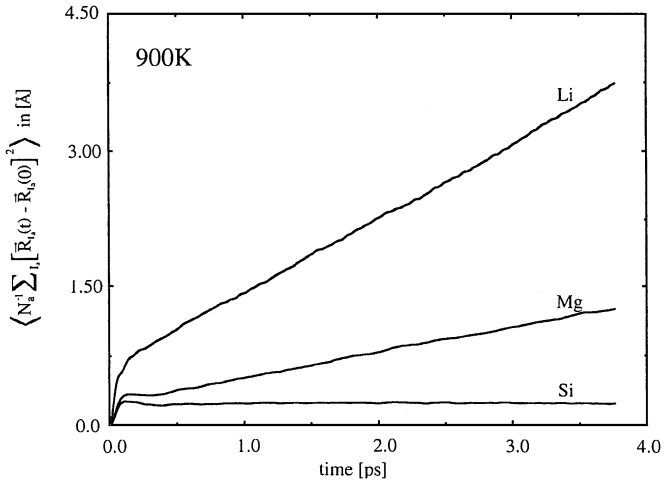


FIG. 8. Mean square displacements of Li, Mg, and Si at 900 K as a function of time. Reprinted with permission from Wengert *et al.* (1996).

Using the Einstein relation,

$$D = \lim_{t \to \infty} \frac{\langle R^2(t) \rangle}{6t}, \tag{24}$$

the diffusivities of Li, Mg, and Si were determined to be $1.4 \times 10^{-5}$, $0.5 \times 10^{-5}$, and $0.0 \times 10^{-5}\,\mathrm{cm}^2/\mathrm{s}$, respectively. It can also be noted in the plots that the linear, diffusive regime was reached at short times (<1 ps). For diffusion that occurs via hopping of large barriers, the time to reach the diffusive regime might be much larger. In this example, the root mean square displacements are small, a few angstroms, over the time scale of the simulations, and one should always be cautious about extrapolating long-time behavior from results over short times. Nevertheless, these values seem reasonable, and Fig. 8 clearly shows that at times above ~0.2 ps, the atoms are no longer moving in an inertial regime.

Molteni *et al.* (1996a) (see also Molteni *et al.,* 1996b) studied the sliding of grain boundaries in germanium using *ab initio* simulations. They simulated the sliding process quasi-statically by shifting the relative positions of two grains and letting the geometry relax after each shift. By this means, they were able to calculate quantitatively the energy as a function of the shear displacement. Figure 9 shows the energy per unit area as a function of the displacement of the grain boundary. They found that the sliding takes place via a stick-slip mechanism, mediated by a rebonding process.

Other studies include the determination of the mechanism of growth of carbon nanotubes (Charlier *et al.,* 1997; Bernholc *et al.,* 1998) and the

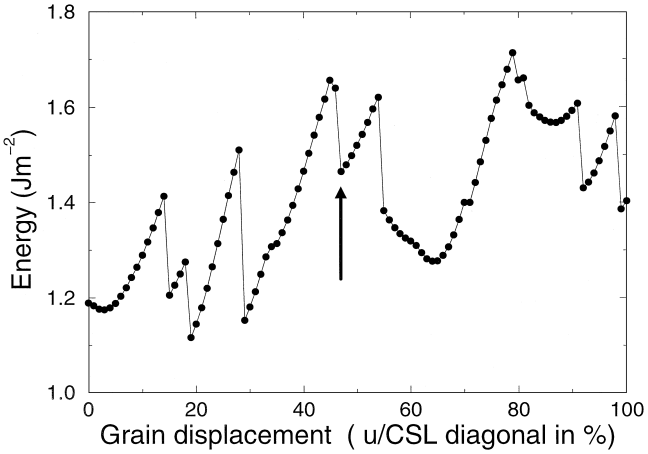


FIG. 9. Grain boundary energy per unit area during the sliding process. The arrow shows where the disorder starts to migrate away from the boundary interface. Reprinted with permission from Molteni *et al.* (1996).

diffusion and motion of various defects in bulk materials (Hamann, 1998; Valladares *et al.,* 1998) including the process of radiation-induced formation of defects (Estreicher *et al.,* 1999). A study by Debernardi *et al.* (1997) used Car–Parrinello simulations to reproduce the essential features of the IR adsorption spectrum of amorphous silicon.

### C. Properties of Liquids, Solvation, and Reactions in Liquids

One of the major objectives of first-principles calculations has been to be able to study liquids. This was not possible before the advent of Car–Parrinello methods, since the disorder of the liquid could not be averaged properly. In recent years, quite a number of studies of reaction processes and structural properties (categories ii and iii) have been performed, primarily on water and on molten metals.

Silvestrelli and Parrinello (1999) studied the structural and bonding properties of liquid water using supercells similar to the one shown in Fig. 2. Note that for computational efficiency, they actually studied $D_2O$. Their work [building on the previous work of Sprik *et al.* (1996)] demonstrates the ability to compute pair correlation functions, as shown in Fig. 10. Comparison with experimental results is extremely good. It should also be noted that there are discrepancies between the two experimental results for the oxygen–oxygen pair correlation curves. (There has been considerable controversy in the literature regarding these curves.)

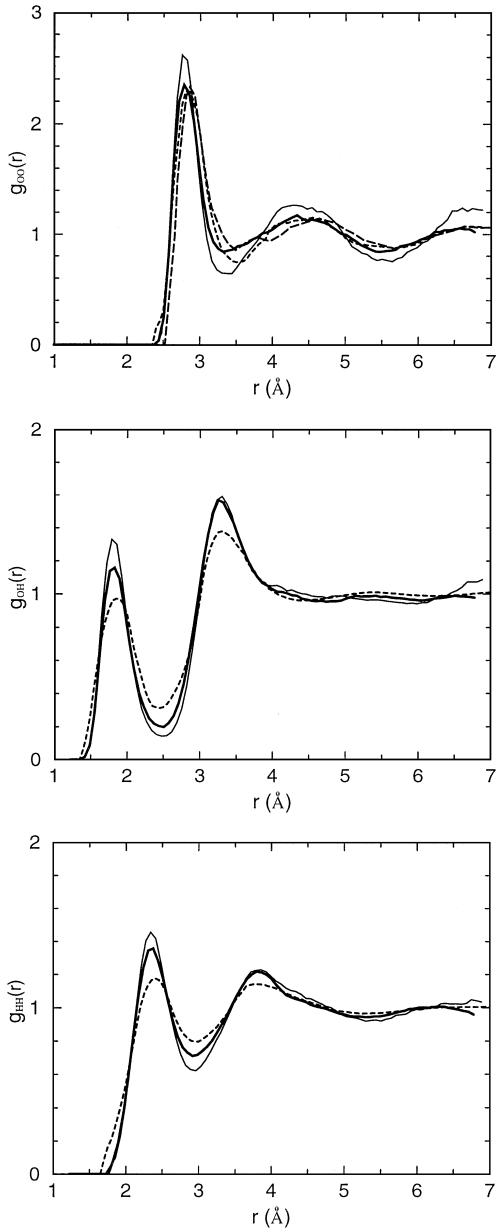


FIG. 10. Pair correlation functions obtained both from Car–Parrinello simulations and from experiments. The thick solid lines are simulation results obtained using a supercell with 64 water molecules. The thin solid lines are for the 32-water molecule simulation. The short-dashed line is from experimental neutron scattering results (Soper *et al.,* 1997), and the long-dashed line is from an X-ray study. Reprinted with permission from Silvestrelli and Parrinello (1999).

In the same study, the diffusivity of water under ambient conditions was determined for the 64-water molecule system to be $2.8 \pm 0.5 \times 10^{-5}$ cm$^2$/s, very close to the experimental value of $2.4 \times 10^{-5}$ cm$^2$/s. Also, the investigators were able to determine the distribution of dipole moments of the water molecules via generation of functions that describe the charge distribution on individual molecules. They found a broad distribution with an average of 3.0 D. This result, aside from being of fundamental scientific significance, has tremendous consequences for modeling of aqueous systems using classical potentials, since in these models the dipole moment of water must be included in the parameterization.

Silvestrelli *et al.* (1997) used Car–Parrinello molecular dynamics to obtain the IR spectrum of $D_2O$. They did so by determining the time autocorrelation function for the dipole moment of their cell and then relating this function to the absorption coefficient as a function of frequency. Their computed spectrum and comparison to experiment are displayed in Fig. 11, taking into account corrections introduced by the authors. The essential features of the experimental spectrum, particularly the low-frequency peak, are reproduced well. The authors were then able to assign specific modes of the spectrum.

This method of computing spectra should be contrasted with the more typical method of calculating harmonic vibrational modes from quantum calculations performed at 0 K. The latter method cannot be applied to liquid systems for which a single, static configuration will not properly describe the system. In addition, the method of Silvestrelli *et al.* (1997) incorporates anharmonic contributions and allows the computation of the IR spectrum directly from the motions of the dipole moment, instead of from nuclear vibrations. While computing IR spectra from first principles in this way is not yet entirely straightforward, Silvestrelli *et al.* (1997) have shown that accurate computations are possible, in addition to demonstrating the power of Car–Parrinello simulations to deconvolute the peaks and to assign them to specific modes.

Other work has been performed in liquid systems, including studying homogeneous catalytic processes, the transport of hydronium and hydroxyl ions in water, reactions in water, the solvation of ions in water, the structure of water/solid interfaces, and the viscosities of liquids.

Woo *et al.* (1997b) used Car–Parrinello molecular dynamics to calculate the free energy barriers for chain termination and chain branching processes during the polymerization of olefins on homogeneous constrained geometry catalysts. Later, the same authors used hybrid methods to study various other homogeneous polymerization catalysts (Woo *et al.,* 1997a). Aagaard *et al.* (1998) studied the reaction mechanism of a ruthenium-based metathesis catalyst, lending support to a mechanism proposed in the literature for the process.

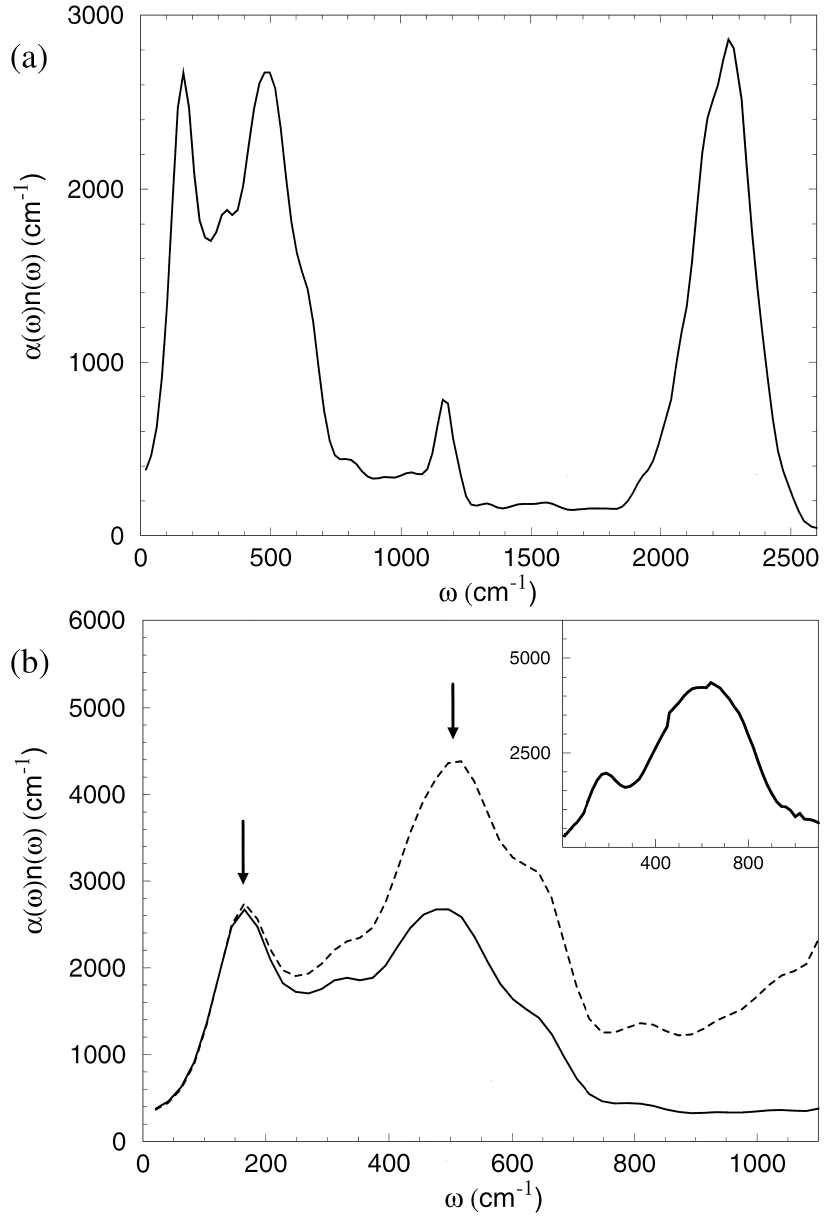


FIG. 11. (a) Computed IR adsorption spectrum of $D_2O$. (b) Comparison of the computed IR adsorption spectrum with experiment. The solid line is the computed spectrum, the dashed line is the computed spectrum with Egelstaff quantum corrections, and the inset shows an experimental IR spectrum of $H_2O$. Reprinted with permission from Silvestrelli *et al.* (1997).

Tuckerman *et al.* (1995) used a 32-water molecule system to investigate the structure and dynamics of proton transfer in aqueous systems at ambient conditions. For hydronium ions, they found dynamic ion complexes, which fluctuated between an $(H_5O_2)^+$ structure and an $(H_9O_5)^+$ structure. For hydroxyl ions, they found that the predominant structure is a fourfold coordinated and planar $(H_9O_5)^-$ complex. They found, however, that proton transfer occurs only via an $(H_7O_4)^-$ complex. They also estimated activation barriers to proton hopping, which are consistent with experimentally observed barriers. The fourfold planar coordination of hydroxyl came as a surprise, since this structure causes the hydrogen bonding network of water to be distorted. Trout and Parrinello (1999) explained this via electron localization arguments.

Liu *et al.* (1999a) studied the hydrolysis of $Cl_2$ in water, while Meijer and Sprik (1998a) investigated the reaction mechanism of water with formaldehyde in sulfuric acid. Laasonen and Klein (1997) studied the hydrolysis of HCl upon addition to water, and Meijer and Sprik (1998b) studied the addition of $H_2O$ to $SO_3$ in solution. Finally, Trout and Parrinello (1998) evaluated the mechanism and free energy profile of the dissociation of $H_2O$ in water.

The solvation of several ions in water has been investigated, including $K^+$ (Ramaniah *et al.,* 1999), $Cu^{2+}$ (Berces *et al.,* 1999), and $Be^{2+}$ (Marx *et al.,* 1997). The structure of a water/silicon interface was studied (Ursenbach *et al.,* 1997), in addition to a water/copper interface (Halley *et al.,* 1998) and a water/palladium interface (Klesing *et al.,* 1998). Finally, two studies have used Car–Parrinello simulations in conjunction with the Green–Kubo relations to calculate viscosities in liquid metals (Alfe and Gillan, 1998; Stadler *et al.,* 1999).

### D. Heterogeneous Reactions and Processes on Surfaces

There has been a variety of studies using Car–Parrinello simulations to determine the structure and energetics of adsorbates on semiconductor and insulating surfaces. Studies on metal surfaces are much rarer, and as far as I know, first-principles molecular dynamics simulations have not yet been used to study reactive processes on metals. The reason is primarily one of computational expense, because metals require the inclusion of a large number of k-points. There is, of course, a substantial body of work which uses static quantum mechanical calculations to study reactions on metal surfaces.

In this section, I have chosen to focus on two case studies of heterogeneous catalytic reaction processes. These fall under category iii, as defined above. The first one involves polymerization reactions on

Ziegler–Natta catalysts. The second one involves hydrocarbon coupling in the solid acid zeolite chabazite.

Boero *et al.* (1998) used Car–Parrinello molecular dynamics to study the polymerization of ethylene at titanium sites in $MgCl_2$-supported Ziegler–Natta catalysts. Their objectives were to evaluate the reaction mechanism, in addition to determining the free energy profile of the polymerization process. Obviously, the characteristic time scale of this process is much greater than the picosecond time scale directly accessible by the simulation. Thus, it is not possible to observe the polymerization process via a straightforward Car–Parrinello simulation.

To circumvent this problem of time scales, Boero *et al.* (1998) used a method of sampling the derivative of the free energy with respect to a reaction coordinate along a reaction pathway. They then integrated this curve to obtain the free energy profile for the reaction. This procedure is called the method of constraints within the "blue moon" ensemble (Carter *et al.,* 1989). The authors chose the initial step in the polymerization process to be the addition of an ethylene molecule to a methyl group bound to the Ti site in the catalyst. Thus, a natural reaction coordinate to choose is the distance between a carbon atom from the ethylene molecule and the carbon atom in the methyl group. With this simple distance constraint, the derivative of the free energy is

$$\frac{dF}{dr_{\mathrm{C–C}}} = -\langle f \rangle_{r_{\mathrm{C–C}}}, \tag{25}$$

where $F$ is the free energy, $r_{\mathrm{C–C}}$ is the value of the constraint, and $\langle f \rangle_{r_{\mathrm{C–C}}}$ is the ensemble averaged force on the constraint, which is equivalent to the ensemble averaged Lagrange multiplier associated with the constraint in the equations of motion. Note that almost any constraint can be chosen as the reaction coordinate, but the resulting equation may be much more complicated than Eq. (24) (Sprik and Ciccotti, 1998).

Initially, Boero *et al.* (1998) performed an optimization of their entire system on a sixfold coordinated Ti site called the Corradini site. They then varied the values of their reaction coordinate, decreasing it by increments of 0.2 to 0.1 Å. At each value of the reaction coordinate, they performed Car–Parrinello simulations to obtain $\langle f \rangle_{r_{\mathrm{C–C}}}$. The temperature of the simulations was 323 K.

The resulting free energy profile is displayed in Fig. 12. Also included in the figure is the total energy calculated at each point. The energy barrier of 14.8 kcal/mol can be compared to experimental estimates of between 6 and 12 kcal/mol. The computed energy of reaction of −6 kcal/mol, however, was much less negative than the experimental estimates of −22 kcal/mol. This discrepancy led the authors to test other sites for their possible catalytic

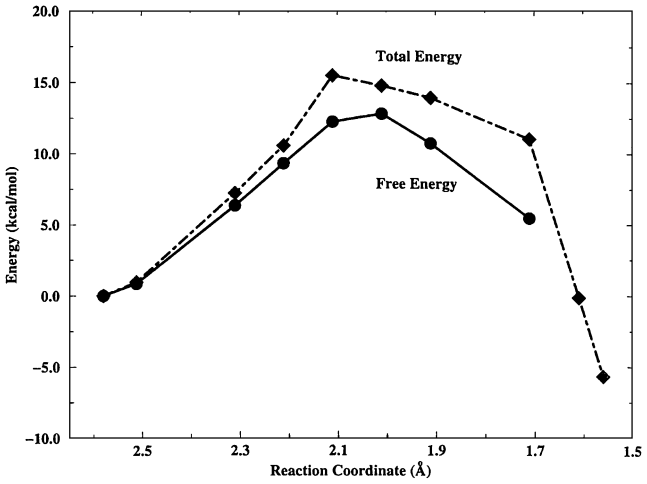


FIG. 12. Free energy and total energy profiles for the insertion of ethylene at the sixfold Corradini site. Reprinted with permission from Boero *et al.* (1998).

activity, including a fivefold coordinated Ti site. The results of energy calculations for this site compared with the sixfold coordinated site are displayed in Fig. 13. The barrier height for the reaction over the fivefold coordinated site is significantly lower than that of the sixfold coordinated site. In addition, the computed energy of reaction matches the measured one. Thus, the authors

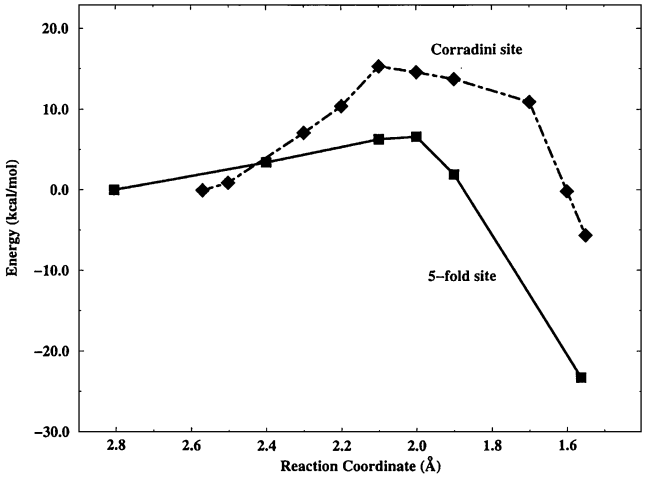


FIG. 13. Comparison of the total energy profiles for the sixfold Corradini site and the fivefold site. Reprinted with permission from Boero *et al.* (1998).

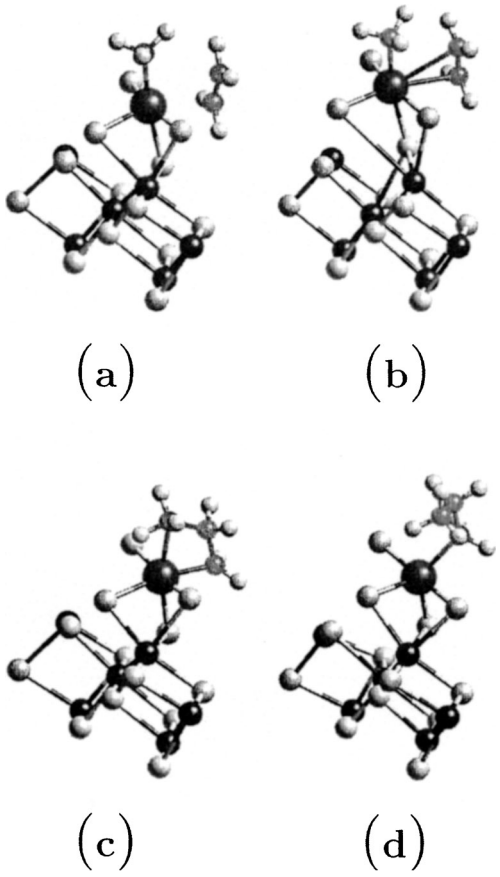


FIG. 14. Snapshots of important steps of the ethylene insertion process over the fivefold Ti site: (a) the approach of the ethylene, (b) formation of the $\pi$-complex, (c) the transition state, and (d) the formed chain. Reprinted with permission from Boero *et al.* (1998).

concluded that the fivefold coordinated site was the active one. Snapshots of the polymerization over the fivefold coordinated site are displayed in Fig. 14.

In our laboratory, we have studied the coupling of two methanol molecules at the acid site of chabazite (see Fig. 1) (Giurumescu and Trout, 2001). This is hypothesized to be an important elementary step in the formation of the first carbon–carbon bond in methanol-to-olefins processes. Because this step has a significant activation barrier, we have chosen to use the method of constraints, with the constraint being the carbon–carbon distance. Simulations were performed at 673 K for 1.5 ps at each point. Our free energy profile is shown in Fig. 15.

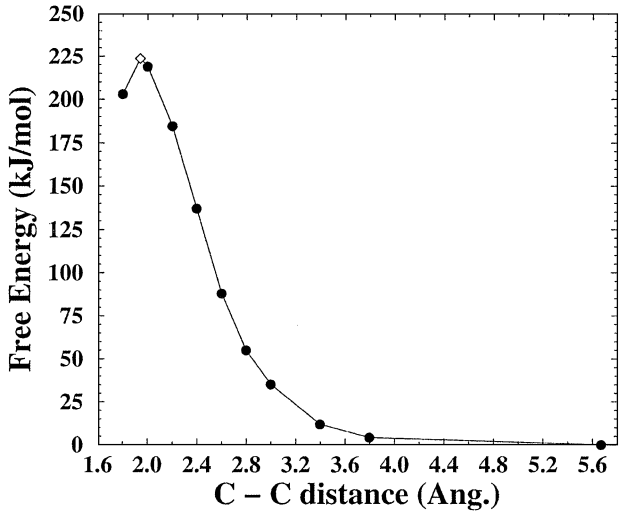


FIG. 15. Free energy profile of carbon–carbon bond formation between two methanol molecules in chabazite. The transition state, found via interpolation, is marked with an open circle.

Aside from quantifying the energetics and the free energy profile for this elementary acid-catalyzed process, we were able to show (1) that the zeolite stabilizes charged complexes, allowing them to move through the channels at 673 K, and (2) a plausible pathway for the reaction process. An important step along the reaction pathway is the formation of a methane-like species and a protonated formaldehyde, both associated with a water molecule. This complex is shown in Fig. 16, slightly before the transition state. As the final stage of the reaction proceeds, the methane-like species transfers a proton to the water molecule in a concerted process through the protonated formaldehyde. The resulting hydronium species moves away as the two remaining species form ethanol. At the very end, the hydronium transfers a proton to the ethanol molecule as it adsorbs at the acidic site, adjacent to the Al atom.

## E. PHASE TRANSITIONS

Car–Parrinello simulations present powerful ways to study phase diagrams and to find new phases of materials, particularly at high pressures. Typically, $(N,T,P)$ simulations are performed using deformable supercells. Methodology can be found in the following references: Focher *et al.* (1994),

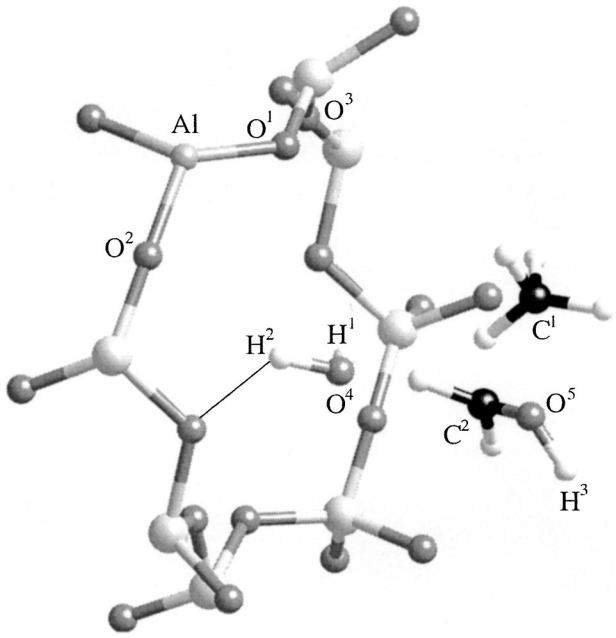


FIG. 16. Configuration close to the transition state, just before concerted proton transfer to the water molecule.

Bernasconi *et al.* (1995), and Bernasconi *et al.* (1996). An example of a relevant phase transition is the polymerization of acetylene under pressure (Bernasconi *et al.,* 1997).

In this study, the authors used a 16-molecule cell, equilibrating it at 298 K and 3 GPa. They then increased the pressure at a rate of 25 GPa/ps, until reaching 9 GPa. At this pressure, they increased the temperature to 400 K and then stepped the pressure to 25 GPa. They observed the polymerization process as shown by the snapshots in Fig. 17. Polymerization did not start until the pressure was increased to 25 GPa. At that pressure, the molecules rapidly formed dimers as shown in Fig. 17b. The final product, shown in Fig. 17c, was a mixture of chains of *cis*- and *trans*-polyacetylene. The authors also analyzed the electronic and energetic characteristics of the system and predicted that the injection of triplet excitons would greatly enhance the rate of polymerization.

Two important studies have predicted the melting point of solid materials from first-principles calculations. Sugino and Car (1995) used Car–Parrinello molecular dynamics to estimate the melting point of silicon from first

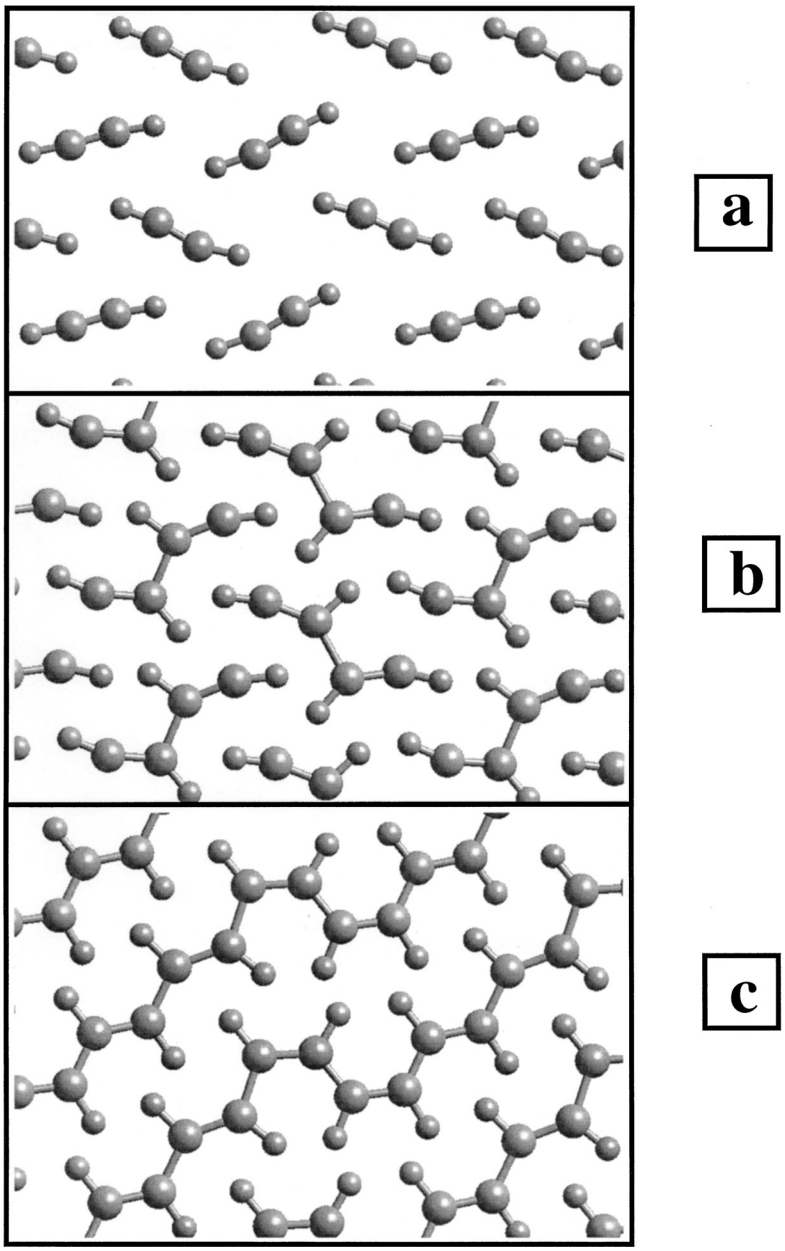


FIG. 17. Pressure-induced polymerization of acetylene. Snapshots of one plane: (a) 9 GPa and 400 K, (b) intermediate configuration at 25 GPa and 400 K, and (c) final configuration at 25 GPa and 400 K. Reprinted with permission from Bernasconi *et al.* (1997).

principles. Their computed value is 1350 K, compared with an experimental value of 1685 K. de Wijs *et al.* (1998) calculated the melting point of Al to be 890 K, compared to an experimental value of 933 K. Because of hysteresis, the computational time necessary to determine the melting points from direct simulations of the melting process is prohibitive. Thus, both groups of authors used thermodynamic integration to compute the free energies of both the liquid and the solid phases as functions of temperatures. The temperature at which these two curves intersect is the melting point.

Even using this approach, the time necessary to compute the free energy at each temperature from Car–Parrinello simulations would be prohibitive. Thus, both groups of authors used two sets of integration calculations. They used classical pair-potential calculations within the scheme of thermodynamic integration to determine the solid and liquid free energy curves, and at each temperature, they used thermodynamic integration to determine the free energy difference between the quantum mechanical system and the classical system.

Another triumph of Car–Parrinello simulations applied to phase transitions was the prediction of a new high-pressure phase of ice, ice XI (Benoit *et al.,* 1996). Other studies include the prediction of a new phase of amorphous silica (Wentzcovitch *et al.,* 1998), the investigation of phase IV of $H_2S$ (Rousseau *et al.,* 1999) and of various phases of HBr (Ikeda *et al.,* 1999), the study of the polymerization of CO under pressure (Bernard *et al.,* 1998), and the study of the phase diagram of carbon at high temperatures and pressures (Grumbach and Martin, 1996). Finally, several studies have isolated metal–insulator transitions in bulk materials (Silvestrelli *et al.,* 1996), and one has investigated the ferroelastic transition in $SiO_2$ stishovite (Lee and Gonze, 1997).

### F. Processes in Biological Systems

On the frontier of Car–Parrinello simulations is the application to biological systems. These systems are large and often require the incorporation of solvation structures, and energetics of solvation are generally important. Thus, computations of entire biomolecules would be too expensive. Nevertheless, several recent studies have isolated essential features of biological processes by studying carefully chosen models consisting of a tractable number of atoms.

A comprehensive review of the state of applying Car–Parrinello simulations to biological simulations has recently appeared (Carloni and Rothlisberger, 2001). For the purpose of this section, I illustrate the kind of models used and the potential of Car–Parrinello methods applied to biological

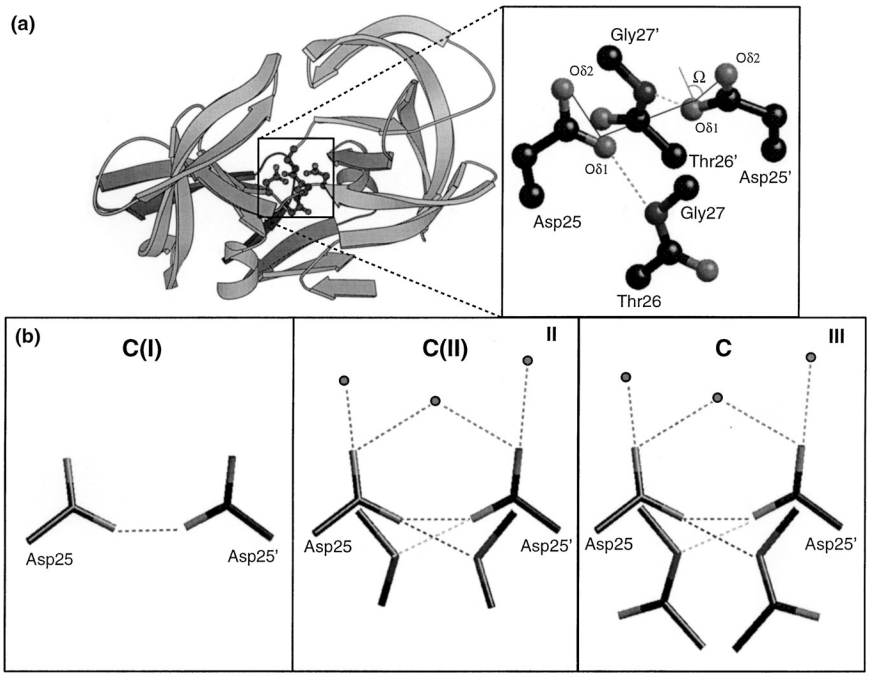


FIG. 18. (a) The structure of HIV-1 PR and its cleavage site; (b) models used in the Car–Parrinello simulations. Reprinted with permission from Carloni and Rothlisberger (2001).

systems, by describing an example of understanding processes in enzymes as a step in developing pharmaceuticals. In particular, the example is chosen from a recent study on HIV-1 protease (Piana and Carloni, 2000).

The structure of this protease is shown in Fig. 18a, including what is thought to be a crucial region for enzymatic function and for the binding of both substrate and inhibitors. Figure 18b shows several models chosen by Piana and Carloni (2000) to study via Car–Parrinello simulations. Figure 19 shows the dynamics of proton motion in the aspartyl dyad for the various models in Fig. 18b. As shown in Fig. 19b, for the C(I) model, the proton can hop between the two oxygen atoms, keeping them close to each other, but the authors conclude that the repulsion of the other oxygen atoms on the carboxylates renders the system unstable.

As shown in Fig. 19c, the choice of model C(II), with water molecules, to model the inclusion of the hydrogen bonding interactions with the neighboring glycines leads to an unstable system. Including the peptide link in model C stabilizes the system, as shown in Fig. 19d, and leads to the conclusion that the strong dipoles of the Thr26(26′)–Gly17(17′) units interact with the

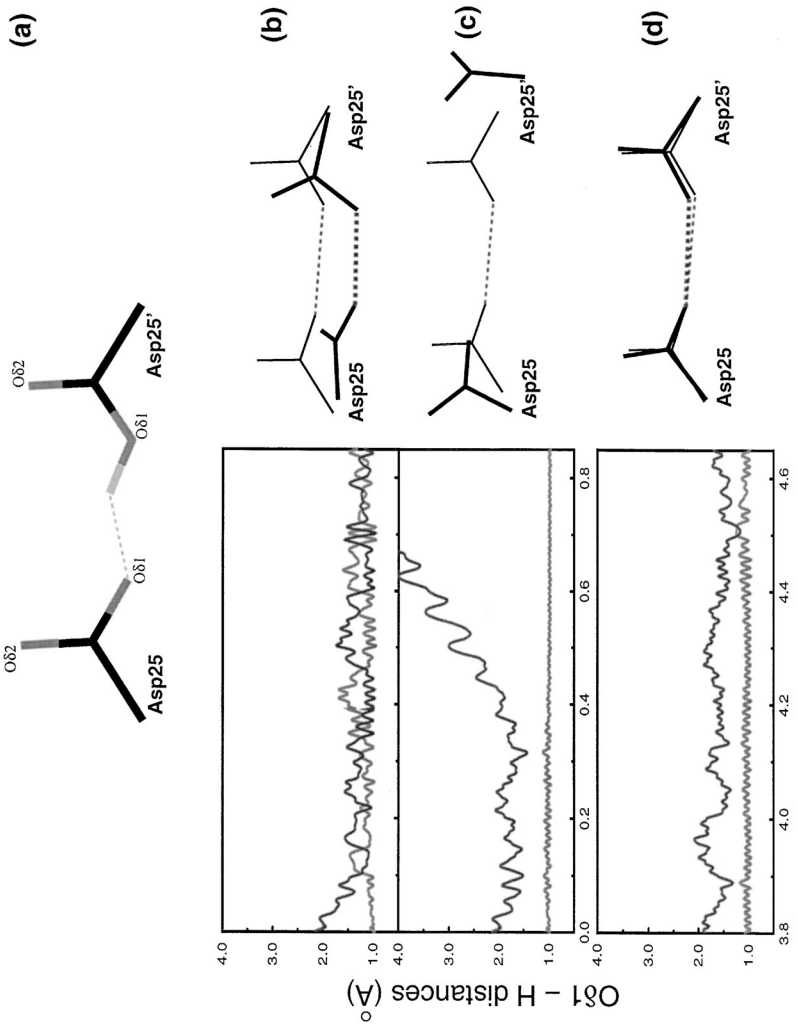


FIG. 19. (a) Location of the proton between the Asp dyad; (b, c, d) position of the proton as a function of time for models C(I), C(II), and C, respectively. Note that in d, only the last 0.9 ps is shown. Reprinted with permission from Carloni and Rothlisberger (2001).

negative charge of the aspartyl dyad, leading to stabilization. Thus, a careful choice of models and simulations by Piana and Carloni (2000) has led to fundamental insight into the stability of an important site of a medically relevant protease.

## VI. Advances in Methodology

Advances in methodology fall into two categories: (1) new algorithms and methods for enhanced computational accuracy and/or performance and (2) ways of incorporating new physics. In terms of category 1, an important direction is the incorporation of classical mechanical potentials within the Car–Parrinello framework so that larger models can be treated, albeit without performing fully quantum mechanical simulations (Woo *et al.,* 1997a, 1999; Rothlisberger, 1998). Thus, for example, many water molecules in a solvated system can be treated classically without much loss in accuracy but with a tremendous gain in speed. Another direction is to use hybrid basis functions, such as a combination of localized functions (e.g., Gaussians) with delocalized functions (e.g., plane waves) (Lippert *et al.,* 1997, 1999). In this way, the advantages of plane waves can be combined with functions that more realistically treat the core regions, where electronic density gradients are large. Another recently proposed scheme is adaptive control of the fictitious orbital mass, $\mu$ in Eqs. (21) and (22), to minimize error and maximize efficiency of each time step of a Car–Parrinello simulation (Bornemann and Schutte, 1999).

Two examples of advanced methodologies which incorporate new physics are the fully quantum mechanical treatment of the nuclei, in addition to the electrons, and the treatment of dynamics on excited state surfaces. A quantum mechanical treatment of the nuclei can be accomplished via the incorporation of path integral methods into the Car–Parrinello scheme (Marx and Parrinello, 1996; Tuckerman *et al.,* 1996). Of course, these methods are useful mainly for treating small systems containing hydrogen atoms. A few applications include the investigation of the $H_5O_2^+$ molecule (Tuckerman *et al.,* 1997), the $CH_5^+$ molecule (Marx and Parrinello, 1999), and solid high-pressure phases of ice (Benoit *et al.,* 1998a, 1999).

A disadvantage of using Car–Parrinello path integral methods is that the molecular dynamics is used only to compute averaged properties, the simulation dynamics having no direct physical meaning. A recently developed, albeit approximate method for generating fully quantum mechanical dynamics is the *ab initio* centroid molecular dynamics method (Marx *et al.,* 1999; Pavese *et al.,* 1999). The application of Car–Parrinello methods to

treat excited state surfaces is extremely recent (Bittner and Kosov, 1999) but promises to become continually more prevalent.

## VII. Concluding Remarks

We have seen the potential and possibilities of Car–Parrinello methods through examples in numerous fields including catalysis, gas- and liquid-phase chemistry, materials, microelectronics, phase behavior, and biology. Via exposure to these examples, which illustrate the state of the art of computational quantum mechanical methods, we can easily see how relevant Car–Parrinello methods are to chemical engineering, which continually demands more detailed understanding of complex molecular processes. I close by reiterating that chemical engineers have always been molecular engineers dealing with complex systems, and we have always been concerned with multiple scales. Not only is the time ripe for chemical engineers to embrace the use of Car–Parrinello methods, but also we are in the ideal position to make new contributions to the development of these methods for the broader engineering and scientific communities.

## APPENDIX A: FURTHER READING

A comprehensive overview of quantum mechanics is given by Cohen-Tannoudji *et al.* (1977), and another good book is by Levine (2000). A staple text on solid-state physics is by Ashcroft and Mermin (1976). A thorough introduction to density-functional theory is given by Parr and Yang (1989). Two good books to learn more about molecular dynamics simulations are by Allen and Tildesley (1987) and Frenkel and Smit (1996). To learn more about pseudopotential methods, two sources with which to begin are by Pickett (1989) and Bachelet *et al.* (1982).

Several reviews on Car–Parrinello molecular dynamics have appeared recently. A comprehensive, book-sized review, focusing on the code developed by Parrinello and collaborators is by Marx and Hutter (2000). Two other good reviews are by Galli and Parrinello (1991) and Galli and Pasquarello (1993). A terse review, focusing on methodology is by Sandré and Pasturel (1997). Other reviews which combine theory with applications are by Parrinello (1997), Gillan (1997), and Radeke and Carter (1997). A review of Car–Parrinello applied to biological systems by Carloni and Rothlisberger (2001) has just appeared.

## APPENDIX B: CODES WITH CAPABILITIES TO PERFORM CAR–PARRINELLO MOLECULAR DYNAMICS

Codes that have Car–Parrinello molecular dynamics implemented are CPMD (Hutter *et al.,* 1995–1999), CASTEP (Molecular Simulations, Inc.), VASP (Kresse and Furthmuller, 1996), HONDO 96 (Dupuis *et al.*), CP-PAW (Blöchl, 1994), fhi98md (Bockstedte *et al.,* 1997), and NWChem (developed and distributed by Pacific Northwest National Laboratory). There are likely many others that have been developed in research laboratories around the world.

## ACKNOWLEDGMENTS

First and foremost, I acknowledge Michele Parrinello, without whom this article would not have been conceived. I also thank those who have helped to teach me both the theory and the practice of Car–Parrinello methods: M. Bernasconi, M. Boero, J. Hutter, D. Marx, C. Moleni, R. Rousseau, C. Rovira, P. Silvestrelli, and M. Tuckerman. Finally, praise for help with the literature search goes to P. Wen and J. Thompson.

## REFERENCES

Aagaard, O. M., Meier, R. J., and Buda, F., *J. Am. Chem. Soc.* **120,** 7174–7182 (1998).

Alfe, D., and Gillan, M. J., *Phys. Rev. Lett.* **81,** 5161–5164 (1998).

Allen, M. P., and Tildesley, D. J., *Computer Simulation of Liquids,* Oxford University Press, Oxford, 1987.

Ashcroft, N. W., and Mermin, N. D., *Solid State Physics,* Saunders College, Philadelphia, 1976.

Bachelet, G. B., Hamman, D. R., and Schluter, M., *Phys. Rev. E* **26,** 4199–4228 (1982).

Becke, A. D., *Phys. Rev. A* **38,** 3098 (1988).

Benoit, M., Bernasconi, M., and Parrinello, M., *Phys. Rev. Lett.* **76,** 2934–2936 (1996).

Benoit, M., Marx, D., and Parrinello, M., *Comput. Mater. Sci.* **10,** 88–93 (1998a).

Benoit, M., Marx, D., and Parrinello, M., *Nature* **392,** 258–261 (1998b).

Benoit, M., Marx, D., and Parrinello, M., *Solid State Ion.* **125,** 23–29 (1999).

Berces, A., Nukada, T., Margl, P., and Ziegler, T., *J. Phys. Chem. A* **103,** 9693–9701 (1999).

Bernard, S., Chiarotti, G. L., Scandolo, S., and Tosatti, E., *Phys. Rev. Lett.* **81,** 2092–2095 (1998).

Bernasconi, M., Chiarotti, G. L., Focher, P., Scandolo, S., Tosatti, E., and Parrinello, M., *J. Phys. Chem. Solids* **56,** 501–505 (1995).

Bernasconi, M., Benoit, M., Parrinello, M., Chiarotti, G. L., Focher, P., and Tosatti, E., *Phys. Scripta* **T66,** 98–101 (1996).

Bernasconi, M., Chiarotti, G. L., Focher, P., Parrinello, M., and Tosatti, E., *Phys. Rev. Lett.* **78,** 2008–2011 (1997).

Bernholc, J., Brabec, C., Nardelli, M. B., Maiti, A., Roland, C., and Yakobson, B. I., *Appl. Phys. A Mater. Sci. Process.* **67,** 39–46 (1998).
Bittner, E. R., and Kosov, D. S., *J. Chem. Phys.* **110,** 6645–6656 (1999).
Blöchl, P. E., *Phys. Rev. B Condensed Matter* **50,** 17953–17979 (1994).
Bockstedte, M., Kley, A., Neugebauer, J., and Scheffler, M., *Comput. Phys. Commun.* **107,** 187–222 (1997).
Boero, M., Parrinello, M., and Terakura, K., *J. Am. Chem. Soc.* **120,** 2746–2752 (1998).
Boese, A. D., Doltsinis, N. L., Handy, N. C., and Sprik, M., *J. Chem. Phys.* **112,** 1670–1678 (2000).
Bornemann, F. A., and Schutte, C., *Numer. Math.* **83,** 179–186 (1999).
Car, R., and Parrinello, M., *Phys. Rev. Lett.* **55,** 2471 (1985).
Carloni, P., and Rothlisberger, U., In *Theoretical Biochemistry—Process and Properties of Biological Systems* (L. Eriksson, ed.), Elsevier Science, Amsterdam, 2001.
Carter, E. A., Ciccotti, G., Hynes, J. T., and Kapral, R., *Chem. Phys. Lett.* **156,** 472 (1989).
Charlier, J. C., DeVita, A., Blase, X., and Car, R., *Science* **275,** 646–649 (1997).
Cohen-Tannoudji, C., Diu, B., and Laloe, F., *Quantum Mechanics,* John Wiley & Sons, New York, 1977.
Curtiss, L. A., Raghavachari, K., Redfern, P. C., and Pople, J. A., *J. Chem. Phys.* **106,** 1063–1079 (1997).
Debernardi, A., Bernasconi, M., Cardona, M., and Parrinello, M., *Appl. Phys. Lett.* **71,** 2692–2694 (1997).
de Wijs, G. A., Kresse, G., and Gillan, M. J., *Phys. Rev. B Condensed Matter.* **57,** 8223–8234 (1998).
Dupuis, M., Marquez, A., and Davidson, E. R., Available from the Quantum Chemistry Program Exchange, Indiana University, Bloomington.
Estreicher, S. K., Hastings, J. L., and Fedders, P. A., *Phys. Rev. Lett.* **82,** 815–818 (1999).
Focher, P., Chiarotti, G. L., Bernasconi, M., Tosatti, E., and Parrinello, M., *Europhys. Lett.* **26,** 345–351 (1994).
Frank, I., Parrinello, M., and Klamt, A., *J. Phys. Chem. A* **102,** 3614–3617 (1998).
Frenkel, D., and Smit, B., *Understanding Molecular Simulations,* Academic Press, San Diego, CA, 1996.
Galli, G., and Parrinello, M., In *Computer Simulations in Materials Science,* Kluwer, Dordrecht, 1991.
Galli, G., and Pasquarello, A., In *Computer Simulation in Chemical Physics,* Kluwer, Dordrecht, 1993.
Gillan, M. J., *Contemp. Phys.* **38,** 115–130 (1997).
Giurumescu, C., and Trout, B. L., in preparation (2001).
Grumbach, M. P., and Martin, R. M., *Phys. Rev. B Condensed Matter* **54,** 15730–15741 (1996).
Haase, F., Sauer, J., and Hutter, J., *Chem. Phys. Lett.* **266,** 397–402 (1997).
Halley, J. W., Mazzolo, A., Zhou, Y., and Price, D., *J. Electroanal. Chem.* **450,** 273–280 (1998).
Hamann, D. R., *Phys. Rev. Lett.* **81,** 3447–3450 (1998).
Hehre, W. J., Radom, L., v. R. Schleyer, P., and Pople, J. A., *Ab Initio Molecular Orbital Theory,* Wiley, New York, 1986.
Hohenberg, P., and Kohn, W., *Phys. Rev.* **136,** B864–B871 (1964).
Hutter, J., Alavi, A., Deutsch, T., Bernasconi, P., Goedecker, S., Marx, D., Tuckerman, M., and Parrinello, M., *CPMD,* version 3.3, MPI für Festkorperforschung and IBM Zurich Research Laboratory, 1995–1999.
Ikeda, T., Sprik, M., Terakura, K., and Parrinello, M., *J. Chem. Phys.* **111,** 1595–1607 (1999).
Janotti, A., Fazzio, A., Piquini, P., and Mota, R., *Phys. Rev. B Condensed Matter* **56,** 13073–13076 (1997).
Kirkpatrick, S., Gelatt, C. D., and Vecchi, M. P., *Science* **220,** 671–680 (1983).

Klesing, A., Labrenz, D., and van Santen, R. A., *J. Chem. Soc. Faraday Trans.* **94,** 3229–3235 (1998).
Kohn, W., and Sham, L. J., *Phys. Rev.* **140,** A1133 (1965).
Kresse, G., and Furthmuller, J., *Phys. Rev. B Condensed Matter* **54,** 11169–11186 (1996).
Laasonen, K. E., and Klein, M. L., *J. Phys. Chem. A* **101,** 98–102 (1997).
Lee, C., Yang, W., and Parr, R. G., *Phys. Rev. B* **37,** 785 (1988).
Lee, C. Y., and Gonze, X., *Phys. Rev. B Condensed Matter* **56,** 7321–7330 (1997).
Levine, I. N., *Quantum Chemistry,* Prentice–Hall, Upper Saddle River, NJ, 2000.
Lippert, G., Hutter, J., and Parrinello, M., *Mol. Phys.* **92,** 477–487 (1997).
Lippert, G., Hutter, J., and Parrinello, M., *Theor. Chem. Acc.* **103,** 124–140 (1999).
Liu, Z. F., Siu, C. K., and Tse, J. S., *Chem. Phys. Lett.* **311,** 93–101 (1999a).
Liu, Z. F., Siu, C. K., and Tse, J. S., *Chem. Phys. Lett.* **314,** 317–325 (1999b).
Marx, D., and Hutter, J., In *Modern Methods and Algorithms of Quantum Chemistry* (J. Grotendorst, ed.), NIC, Forschungszentrum, Julich, 2000, pp. 301–449.
Marx, D., and Parrinello, M., *J. Chem. Phys.* **104,** 4077–4082 (1996).
Marx, D., and Parrinello, M., *Science* **284,** 59 (1999).
Marx, D., Sprik, M., and Parrinello, M., *Chem. Phys. Lett.* **273,** 360–366 (1997).
Marx, D., Tuckerman, M. E., and Martyna, G. J., *Comput. Phys. Commun.* **118,** 166–184 (1999).
Meijer, E. J., and Sprik, M., *J. Am. Chem. Soc.* **120,** 6345–6355 (1998a).
Meijer, E. J., and Sprik, M., *J. Phys. Chem. A* **102,** 2893–2898 (1998b).
Molteni, C., Francis, G. P., Payne, M. C., and Heine, V., *Phys. Rev. Lett.* **76,** 1284–1287 (1996a).
Molteni, C., Francis, G. P., Payne, M. C., and Heine, V., *Mater. Sci. Eng. B Solid State Mater. Adv. Technol.* **37,** 121–126 (1996b).
Papoulias, P., Morgan, C. G., Schick, J. T., Landman, J. I., and Rahhal-Orabi, N., *Defects in Semiconductors, Icds-19, Pts. 1–3* **258**(2), 923–927 (1997).
Parr, R. G., and Yang, W., *Density Functional Theory of Atoms and Molecules,* Oxford University Press, New York, 1989.
Parrinello, M., *Solid State Commun.* **102,** 107–120 (1997).
Pavese, M., Berard, D. R., and Voth, G. A., *Chem. Phys. Lett.* **300,** 93–98 (1999).
Perdew, J. P., and Wang, Y., *Phys. Rev. B* **45,** 13244–13249 (1992).
Perdew, J. P., Burke, K., and Ernzerhof, M., *Phys. Rev. Lett.* **77,** 3865–3868 (1996).
Piana, S., and Carloni, P., *Proteins Struct. Funct. Gen.* **39,** 26–36 (2000).
Pickett, W. E., *Comp. Phys. Rep.* **9,** 115–198 (1989).
Radeke, M. R., and Carter, E. A., *Annu. Rev. Phys. Chem.* **48,** 243–270 (1997).
Ramaniah, L. M., Bernasconi, M., and Parrinello, M., *J. Chem. Phys.* **111,** 1587–1591 (1999).
Raugei, S., Cardini, G., and Schettino, V., *J. Chem. Phys.* **111,** 10887–10894 (1999).
Rothlisberger, U., *J. Mol. Graph.* **16,** 275–276 (1998).
Rousseau, R., Boero, M., Bernasconi, M., Parrinello, M., and Terakura, K., *Phys. Rev. Lett.* **83,** 2218–2221 (1999).
Sandré, E., and Pasturel, A., *Mol. Simul.* **20,** 63–77 (1997).
Silvestrelli, P. L., and Parrinello, M., *J. Chem. Phys.* **111,** 3572–3580 (1999).
Silvestrelli, P. L., Alavi, A., Parrinello, M., and Frenkel, D., *Phys. Rev. B Condensed Matter* **53,** 12750–12760 (1996).
Silvestrelli, P. L., Bernasconi, M., and Parrinello, M., *Chem. Phys. Lett.* **277,** 478–482 (1997).
Soper, A. K., Bruni, F., and Ricci, M. G., *J. Chem. Phys.* **106,** 247 (1997).
Sprik, M., and Ciccotti, G., *J. Chem. Phys.* **109,** 7737–7744 (1998).
Sprik, M., Hutter, J., and Parrinello, M., *J. Chem. Phys.* **105,** 1142–1152 (1996).
Stadler, R., Alfe, D., Kresse, G., de Wijs, G. A., and Gillan, M. J., *J. Non-Cryst. Solids* **250,** 82–90 (1999).
Sugino, O., and Car, R., *Phys. Rev. Lett.* **74,** 1823–1826 (1995).

Szabo, A., and Ostlund, N. S., *Modern Quantum Chemistry,* McGraw–Hill, New York, 1989.
Trout, B. L., and Parrinello, M., *Chem. Phys. Lett.* **288,** 343–347 (1998).
Trout, B. L., and Parrinello, M., *J. Phys. Chem. B* **103,** 7340–7345 (1999).
Tuckerman, M., Laasonen, K., Sprik, M., and Parrinello, M., *J. Chem. Phys.* **103,** 150–161 (1995).
Tuckerman, M. E., Marx, D., Klein, M. L., and Parrinello, M., *J. Chem. Phys.* **104,** 5579–5588 (1996).
Tuckerman, M. E., Marx, D., Klein, M. L., and Parrinello, M., *Science* **275,** 817–820 (1997).
Ursenbach, C. P., Calhoun, A., and Voth, G. A., *J. Chem. Phys.* **106,** 2811–2818 (1997).
Valladares, A., White, J. A., and Sutton, A. P., *Phys. Rev. Lett.* **81,** 4903–4906 (1998).
Wengert, S., Nesper, R., Andreoni, W., and Parrinello, M., *Phys. Rev. Lett.* **77,** 5083–5085 (1996).
Wentzcovitch, R. M., da Silva, C., Chelikowsky, J. R., and Binggeli, N., *Phys. Rev. Lett.* **80,** 2149–2152 (1998).
Woo, T. K., Margl, P. M., Blöchl, P. E., and Ziegler, T., *J. Phys. Chem. B* **101,** 7877–7880 (1997a).
Woo, T. K., Margl, P. M., Ziegler, T., and Blöchl, P. E., *Organometallics* **16,** 3454–3468 (1997b).
Woo, T. K., Margl, P. M., Deng, L., Cavallo, L., and Ziegler, T., *Catal. Today* **50,** 479–500 (1999).
Yamataka, H., Aida, M., and Dupuis, M., *Chem. Phys. Lett.* **300,** 583–587 (1999).